THE FLORIDA STATE UNIVERSITY

COLLEGE OF ARTS AND SCIENCES

TIME AND SPACE VARIABILITY OF TROPICAL PACIFIC WIND STRESS

by

Stanley B. Goldenberg

A Thesis submitted to the
Department of Meteorology
in partial fulfillment of the
requirements for the degree of
Master of Science

Approval:

James J. O'Brien
Professor Directing Thesis

M E LaSeur

C L Jordan

[illegible]

[illegible]

March, 1980

ABSTRACT

The results of a spectral analysis of a new, subjectively analyzed data set of tropical Pacific wind stress are presented. The monthly data for the 10 year period, 1961-1970, allows a detailed inspection of the distributions of frequency and zonal wavenumber spectra from 29°N to 29°S. In addition, the subjective analysis technique is briefly compared with two objective methods.

The frequency spectra vary greatly throughout the tropical Pacific. There are also differences between the spectra for the wind stress magnitude and its components. The only statistically significant peaks are for the annual and semiannual cycles. The differences between the frequency spectra for the wind stress magnitude and the wind stress components are discussed. Plots of the spatial distributions of the power in the annual and semiannual signals are presented and related to seasonal climatological features in the tropical Pacific wind field. Other plots are introduced which show regions of high interannual variability in the area occupied by the Southern Oscillation, and in the central equatorial Pacific. Both of these regions are key areas in the study of El Niño.

Zonal wavenumber spectra are presented as functions of latitude for January, February, etc. The spectra are red, as would be expected.

for January, February, etc. The spectra are red, as would be expected.

The outcome of a test for white noise, that was performed on the frequency spectra for interannual periods is discussed. According to the data set used in this study, the spectra are indistinguishable from white spectra for interannual periods. However, the results for this type of test are hindered by the short record length available in the data set.

ACKNOWLEDGEMENTS

I would like to express my sincere appreciation to Dr. James J. O'Brien for serving as my major professor and for his support and encouragement during the course of this research. I reaped many benefits from his vast knowledge and experience. I wish to thank the other members of my committee, Drs. Charles Jordan, Noel LaSeur and Duane Meeter, for their valuable assistance. I also thank Dr. Jesse Stephens for his guidance in performing the objective analysis.

I greatly appreciate all of the time and effort contributed to this research by everyone in the Mesoscale Air-Sea Interaction Group at Florida State. In particular, I wish to thank George Heburn for his help with computer-related problems. I would also like to acknowledge the assistance of Antonio Busalacchi Jr., Monty Peffley, Dale Hawkins, John Klinck, Noreen O'Malley, Dewey Rudd, Sheri Johns, Judy Estes and Sheila O'Brien.

I am very grateful to Susan Finney for typing both the draft copies and the final version of the thesis.

I would like to express my deep appreciation to the many people who helped with the tedious task of creating the data base that was used in this study. In particular, I wish to thank John Allsopp and

used in this study. In particular, I wish to thank John Allsopp and

Robert Davy for their excellent work. I also would like to thank James Green, Linda Koss, Frank Mosely, Holly Jones, LuAnne Schendel, William Psinakis, Peter Larson, Dean Brown, James Jeter and Ronald Goodman for their contributions.

My special thanks goes to Betty Stevens and Amy Mitchell for their support and for the many hours of assistance which they freely gave during this project. I would also like to thank Raymond Kasch, Lawrence Wenzel, John Wilson and Daniel Letton for their help and encouragement.

This work was supported by the Division of Atmospheric Sciences, NSF, under Grant ATM7920485, the CUEA Project of IDOE, NSF, and the Office of Naval Research. Computations were performed on the CDC Cyber 73 and Cyber 74 at the Florida State University.

TABLE OF CONTENTS

e. Distribution of Interannual Variability 40

Table of Contents (continued)

LIST OF TABLES

LIST OF ILLUSTRATIONS

List of Illustrations (continued)

1. INTRODUCTION

In the meteorological community, there has been an increased interest in the tropics as an aid to improve long range weather prediction. A major climatological feature in the tropics is the wind field, because geostrophy is not valid near the equator. Oceanographers are building more complicated ocean models for the tropics. In these, the main driving variable is the wind stress. This study is an attempt to investigate specific aspects of the time and space variability of the wind stress over the tropical Pacific Ocean.

El Niño, a major air-sea interaction event, is believed to be caused by remote forcing in the wind stress over the Pacific Ocean (Wyrtki, 1975; Hurlburt et al., 1976; McCreary, 1976; Kindle, 1979). SCOR Working Group 55, "Prediction of El Niño", has established the definition: "El Niño is a massive intrusion of warm water into the eastern equatorial Pacific with positive coastal sea surface temperature anomalies exceeding 2°C as far south as 12°S" (D.W. Stuart, personal communication).

Willebrand (1978) did one of the most recent studies to investigate the temporal and spatial scales of oceanic winds. He analyzed the quasi-geostrophic wind field over the Pacific and Atlantic Oceans from 20-65°N. The winds were calculated from synoptic-scale surface pressure

20-65°N. The winds were calculated from synoptic-scale surface pressure

data for a four-year period. He also used actual wind observations from two weatherships. He found that, excluding the annual signal, the spectra of the wind stress are "white" (i.e., flat) for periods longer than 10 days.

Unfortunately, in the tropics, it is not possible to obtain accurate winds using the pressure field. Early attempts have made use of ship wind observations to study the mean monthly and annual wind distributions (McDonald, 1938; Crowe, 1951a, b; U.S. Navy Hydrographic Office, 1956; Hellerman, 1967). Wyrtki and Meyers (1975a, b, 1976) have recently processed five million ship wind observations between 30°N and 30°S over the Pacific Ocean for the years, 1900-1973. The data were used to create maps of average monthly winds and wind stresses for 2° x 10° latitude-longitude quadrangles. Wyrtki and Meyers used the data to study both the seasonal and interannual variability of the Pacific Ocean trade wind field. Barnett (1977a) has used the data to investigate the time and space variability of the trades. Reiter (1978a, b) utilized the data to research the interannual changes in the ocean atmosphere system.

The wind stress data for the ten-year period, 1961-1970, were subjectively analyzed and digitized on a 2° x 2° latitude-longitude grid. There were three primary motivations for creating a revised data set:

1) There were obvious errors contained in the original data set;
2) A finer grid was needed to drive coupled atmospheric-ocean models;
3) For many of the months, there were regions entirely void of data. Also, there were many 2° x 10° boxes containing so few

observations that the representativeness of the average monthly values were in question.

The results from the subjective analysis are compared with the results that have been obtained using the objective techniques of optimum interpolation (Goldenberg, 1979, unpublished manuscript) and empirical orthogonal analysis (Barnett, 1977a).

This study uses the digitized data of the subjective analysis to perform a detailed investigation of the distributions of the frequency and wavenumber spectra for the wind stress over the Pacific Ocean. In particular, the power of the semiannual, annual and low frequency (i.e., interannual) signals is discussed as a function of latitude and longitude. The seasonal variability of the wave number spectra is discussed as a function of latitude.

The complete frequency spectra show pronounced annual and/or semiannual peaks for many regions, while for other regions, the spectra are flat. The spectra for the stress magnitude often differ significantly from that of the zonal and meridional components. The distributions of the energy for the annual and semiannual cycles clearly depict the major climatological features, such as the seasonal fluctuations of: the monsoon circulations of southeast Asia and northeast Australia, the strength and position of the intertropical convergence zone (ITCZ), strength of the trades and the intrusions of middle latitude storms into the subtropics.

This study reveals four major areas of large interannual variability in the wind stress field. A band of high energy lies between Chile and Australia. This is the area of the Southern Oscillation which has

been used to forecast El Niño intrusions and abnormally heavy rainfall over the central and western equatorial Pacific (Quinn and Burt, 1970, 1972; Quinn, 1974; Wyrtki et al., 1976). The distribution for the meridional stress component displays high energy along the mean position of the ITCZ to the east of the dateline. Reiter (1978b) has recently demonstrated how the long-term variability in these components is correlated with rainfall amounts along the ITCZ. He also showed how the trends are associated with occurrences of El Niño. The third area of high interannual energy is located in the equatorial Pacific in the vicinity of the dateline. This is an important area in the processes which are believed to cause El Niño events (Wyrtki, 1975; Kindle, 1979; O'Brien, 1979). The other area of high variability is associated with the interannual fluctuations in the severity of the penetration of winter mid-latitude storms into the subtropics. Of particular interest is the absence of large amounts of low frequency energy along the western coasts of North and South America. This last feature is further confirmation of the theory that El Niño is not caused by interannual changes in the local winds (Wyrtki, 1975; Barnett, 1977b; Kindle, 1979; O'Brien et al., 1979).

The zonal wave number spectra, which are calculated along each latitude for the tropical Pacific, produce red spectra, as expected. The spectral estimates are averaged for each month to show seasonal variability. The variance is usually concentrated in the band of GWN 3-12. This is especially true for the latitude bands containing the regions of maximum trade winds or winter storm tracks.

GWN 3-12. This is especially true for the latitude bands containing the regions of maximum trade winds or winter storm tracks.

Some ocean climate models incorporate the assumption that the frequency spectra of the wind stress are white for periods longer than the annual (Frankignoul and Müller, 1979). A test which examines the integrated spectrum as a cumulative distribution function was performed on the spectra for interannual periods. The results support the hypothesis that the spectra are white for low frequencies. However, the significance of this result is limited by the short record length (ten years). A much longer record length is needed to resolve adequately interannual variability.

2. THE DATA BASE

This section will detail the steps that were taken to create the data base of monthly-averaged wind stress values for the tropical Pacific Ocean on a 2° latitude by 2° longitude grid for the ten-year period, January, 1961 - December, 1970. Another attempt to provide wind stress data was by Hellerman (1967), who made use of climatological atlases along with wind-speed frequencies to resolve seasonal wind stress over the world oceans on 5° squares. More recently, Wyrtki and Meyers (1975a, b, 1976) have collected large amounts of ship observations over the tropical Pacific and computed monthly averages of both the wind stress and wind speed in 2° latitude by 10° longitude boxes. This latter data set was subjectively analyzed to provide the data base used for this paper.

a. Original data set

Previous wind stress distributions, such as Hellerman (1967), were resolved only on 5° squares and by season. One of the limitations with the coarse resolution was the inadequate resolution of north-south gradients. Wyrtki and Meyers (1975a, b, 1976), using a larger collection of observations than previously available (five million reports), computed bimonthly averages for the period 1900-1946, and monthly averages for 1947-1973, on a 2° x 10° latitude-longitude grid.

ages for 1947-1973, on a 2° x 10° latitude-longitude grid.

Those observations with speeds greater than 40 m s^{-1} during typhoons were not included in the monthly values. The stresses were computed from individual ship wind observations according to

$$\begin{aligned} \tau &= \rho_a C_D W^2 \\ \tau_x &= \rho_a C_D W_x W \\ \tau_y &= \rho_a C_D W_y W, \end{aligned} \tag{1}$$

where τ is the magnitude of the wind stress, ρ_a is the air density, C_D is the drag coefficient and W is the magnitude of the horizontal wind speed defined by $\underset{\sim}{W} = W_x \hat{i} + W_y \hat{j}$, $W^2 = W_x^2 + W_y^2$. The subscripts x and y refer to the components positive to the east and north, respectively. Constant values were assumed for the drag coefficient, $C_D = 1.5 \times 10^{-3}$, and for the air density, $\rho_a = 1.2$ kg m^{-3}.

b. Subjective analysis technique

The ten-year period, 1961-1970, was chosen for the analysis because it is the period with the most consistent data coverage for the years 1947-1973. Table 1 shows the monthly data coverage during the decade. Fig. 1 shows the overall average monthly data coverage. The data network was excellent to the north of 17°N, and good for most of the Northern Hemisphere. However, almost one-third of the area in the Southern Hemisphere used for this study was a victim of poor coverage. The quantitative results for those regions are probably unreliable. Fig. 2 shows the actual area covered by the subjective analysis. The analysis actually included some land areas, even though the wind stress values were only located over water. The basin was extended to facilitate the
actually included some land areas, even though the wind stress values were only located over water. The basin was extended to facilitate the
approximate land boundaries that are used in ocean models. No addi-

MONTH	YEAR	NOBS < 4	NOBS > 30
1	1961	104	106
2	1961	134	95
3	1961	107	126
4	1961	103	100
5	1961	99	102
6	1961	113	96
7	1961	138	65
8	1961	120	87
9	1961	127	55
10	1961	104	90
11	1961	133	83
12	1961	132	93
1	1962	116	103
2	1962	125	83
3	1962	116	105
4	1962	118	98
5	1962	113	92
6	1962	109	97
7	1962	118	91
8	1962	122	80
9	1962	121	71
10	1962	104	89
11	1962	115	89
12	1962	116	84
1	1963	115	91
2	1963	142	64
3	1963	114	91
4	1963	124	83
5	1963	137	87
6	1963	134	75
7	1963	152	69
8	1963	151	67
9	1963	139	80
10	1963	153	86
11	1963	144	74
12	1963	135	95
1	1964	76	124
2	1964	77	123
3	1964	70	125
4	1964	72	106
5	1964	79	126
6	1964	80	98
7	1964	77	116
8	1964	65	108
9	1964	78	101
10	1964	71	124
11	1964	55	128
12	1964	55	140
1	1965	73	141
2	1965	73	114
3	1965	68	152
4	1965	65	141
5	1965	65	142
6	1965	52	128
7	1965	100	131
8	1965	70	143
9	1965	75	125
10	1965	50	133
11	1965	52	152
12	1965	60	140
1	1966	44	143
2	1966	53	131
3	1966	42	141
4	1966	43	143
5	1966	44	135
6	1966	63	130
7	1966	70	129
8	1966	74	149
9	1966	52	138
10	1966	57	139
11	1966	66	148
12	1966	81	139
1	1967	96	131
2	1967	67	147
3	1967	73	139
4	1967	68	138
5	1967	95	133
6	1967	60	122
7	1967	91	124
8	1967	108	138
9	1967	96	134
10	1967	92	135
11	1967	75	132
12	1967	75	133
1	1968	98	137
2	1968	99	132
3	1968	71	134

Table 1. Number of grid points each month for the period, January, 1961-December, 1970, for which the number of observations (NOBS) was < 4 or > 30.

Table 1 (continued)

MONTH	YEAR	NOBS < 4	NOBS > 30
4	1968	87	143
5	1968	87	123
6	1968	88	130
7	1968	81	126
8	1968	103	136
9	1968	100	131
10	1968	80	145
11	1968	118	118
12	1968	84	127
1	1969	81	135
2	1969	85	140
3	1969	91	154
4	1969	103	130
5	1969	94	137
6	1969	103	127
7	1969	78	142
8	1969	107	130
9	1969	92	127
10	1969	73	139
11	1969	81	140
12	1969	98	139
1	1970	153	120
2	1970	143	115
3	1970	148	130
4	1970	141	116
5	1970	117	126
6	1970	143	118
7	1970	157	111
8	1970	160	107
9	1970	131	112
10	1970	142	108
11	1970	126	113
12	1970	142	107

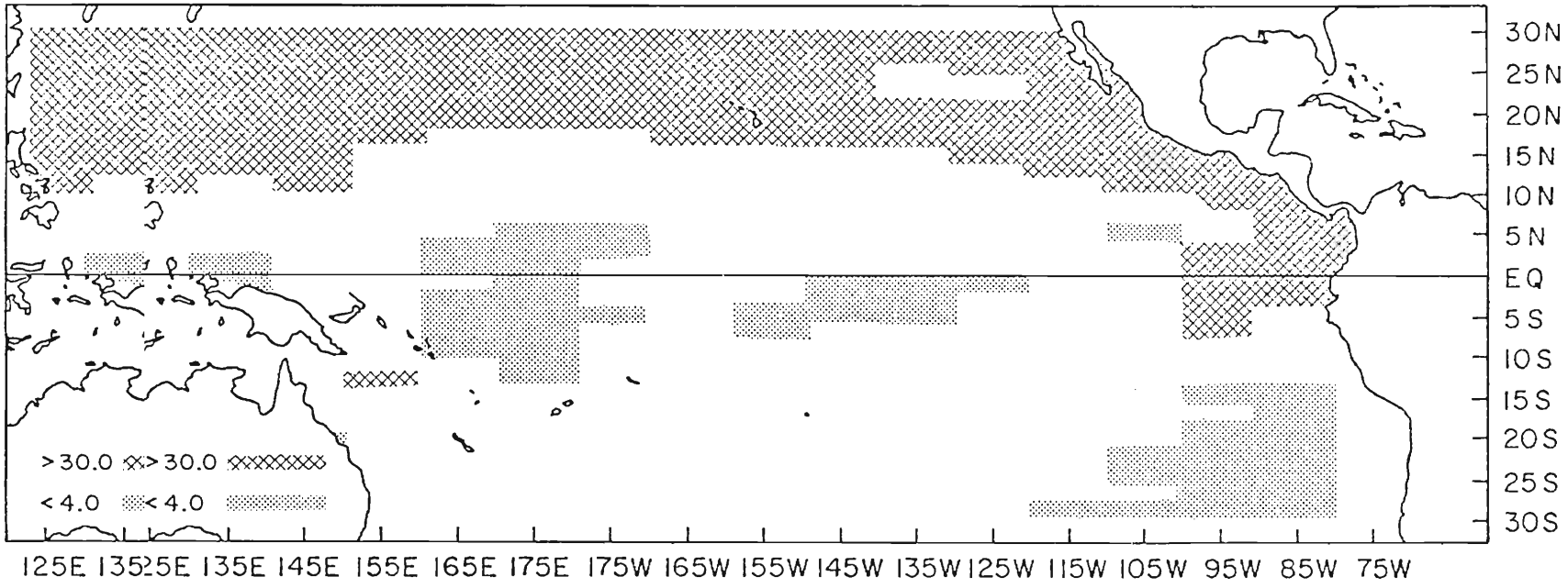

Fi; Fig. 1. Areas where the overall average number of monthly observations was < 4 or > 30 for thefor the ten-year period, January, 1961 - December, 1970.

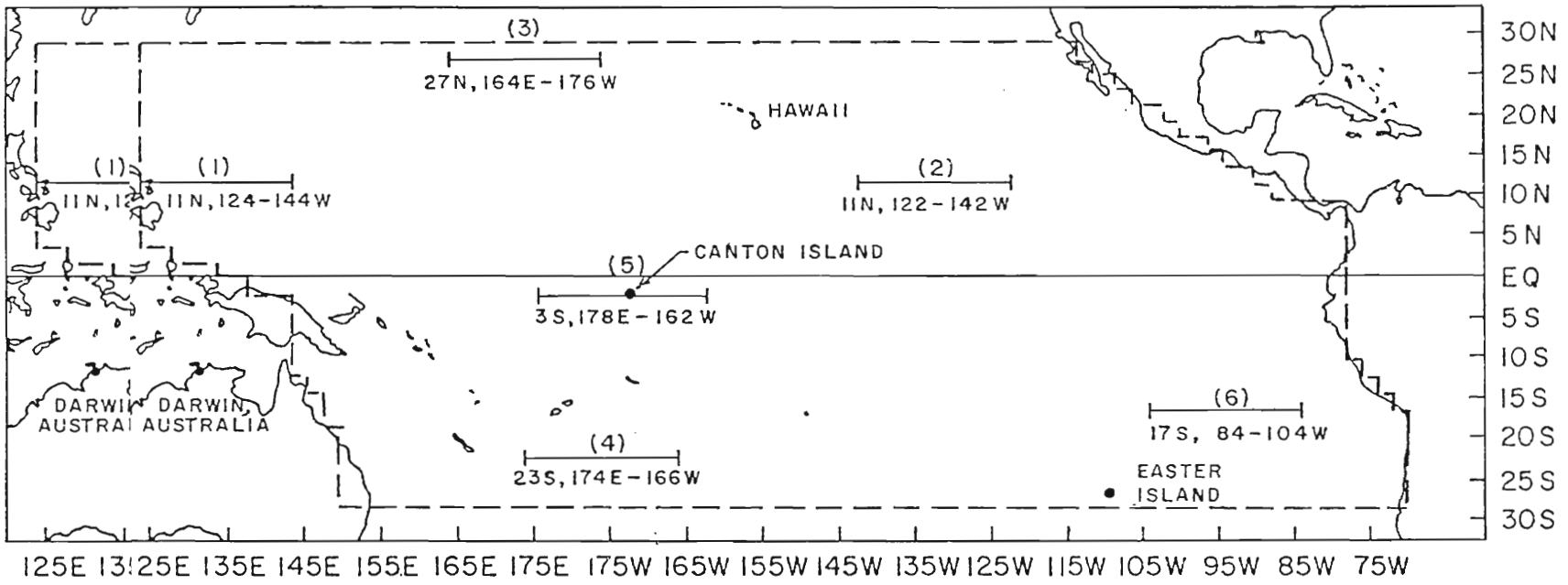

Fi Fig. 2. Subjective analysis "basin" (dashed outline) and locator chart for referenced sites. sites.

tional noise is apparent in the frequency spectra on the boundaries due to this extrapolation. Caution should be exercised however, when using the extrapolated data. Some of the original monthly values were located at grid points over land. For the analysis, each value was assigned to the center of the portion of the 2° x 10° box which was located over water.

The analysis was done by drawing separate scalar analyses of the two components of the wind stress τ_x and τ_y. There were many cases of incorrect or unrepresentative data in the original 2° x 10° set. In addition, there were boxes totally void of data for certain months. Standard synoptic techniques were used, such as climatology (McDonald, 1938; Wyrtki and Meyers, 1975a; Hastenrath and Lamb, 1977), continuity, topography (for boundary regions), etc.

There were several methods for dealing with questionable data. The number of observations (NOBS) in the 2° x 10° boxes varied from zero to several hundred. Therefore, the representativeness of the wind stress values as the actual monthly averages also varied considerably. In the analyses, the observations were weighted according to the NOBS for each box for that particular month. There were several occurrences of obvious sign errors due to bad data transmission. Bimonthly stress vector maps from the original data (Wyrtki and Meyers, 1975b) were used to check for these. In addition, the monthly average values were smoothed if they produced unrealistically strong gradients.

In regions that were void of any data for a particular month, three methods were used to fill in the gaps. First, use was made of the sur-

In regions that were void of any data for a particular month, three methods were used to fill in the gaps. First, use was made of the sur-rounding data and patterns. Second, an attempt was made to use time

continuity from the previous and subsequent maps. Thirdly, climatological maps were used as aids to fill in the gaps.

After the contour maps were drawn, they were digitized using a 2° by 2° grid. There were several checks made on the digitized data to eliminate errors. These controls included: checking the punched cards against the original tabulation sheets, comparing the contour maps drawn by computer of the digitized data with the original contour maps, and checking the vector maps produced from the data for questionable flow fields. Computer printouts of the final data were then compared to the original tabulated data.

The air density, ρ_a, is approximately constant within 30° of the equator. It was demonstrated by Willebrand (1978) that the linear stress law (i.e., C_D = constant) is adequate for a spectral analysis involving periods greater than 10 days. Therefore, the quantity, $\rho_a C_D$, was assumed constant and was not included in the analyses. For the remainder of this paper, the term "wind stress" will refer to the quantities given in (1) without the factor, $\rho_a C_D$, i.e.,

$$\underset{\sim}{\tau} = \tau_x \hat{i} + \tau_y \hat{j}$$
$$\tau^2 = \tau_x^2 + \tau_y^2,$$

where τ_x and τ_y, the zonal and meridional components of the wind stress, respectively, will refer to the quantities

$$\tau_x = W_x W \qquad (2)$$
$$\tau_y = W_y W.$$

(2)

$\tau_y = W_y W.$

c. Subjective versus objective approach

After careful consideration of the alternatives, the subjective mapping approach discussed above was chosen to perform the analysis for this study rather than an objective technique. The original monthly 2° x 10° data have also been analyzed through the use of two objective approaches. Barnett (1977a) used the method of empirical orthogonal functions (EOF). Goldenberg (1979, unpublished manuscript) has analyzed selected months of the original data set using the method of optimum interpolation analysis. The results from these methods will be discussed briefly.

The EOF analysis by Barnett (1977a) covered the years 1950-1972. He chose to deal with the problem of sparse data coverage by using bimonthly, 4° latitude x 10° longitude averages. Some areas of very poor coverage were eliminated. He filled any remaining voids by "space/time interpolation of missing data using the low-order frequency components of the actual data".

The other objective analysis (Goldenberg, 1979, unpublished manuscript) employed the method of successive corrections (MSC) developed by Bergthorssen and Döös (1955) and later expanded by Cressman (1959). An elliptical influence radius, based on the ratios of the average gradients in the x- and y-directions, was used for the analysis. The monthly climatological values (Wyrtki and Meyers, 1975a) were used as first guess fields. Also, as shown by Stephens and Polan (1970), it was necessary to filter out all waves after each scan that cannot be resolved by the average station separation, to prevent numerical insta-was necessary to filter out all waves after each scan that cannot be resolved by the average station separation, to prevent numerical insta-bility. This was a simple, straightforward attempt to apply MSC to the

data. It only covered about 90 percent of the area used in the subjective analysis.

There are no major differences between the subjective and the MSC analyses. However, the MSC objective maps contain less detail in the east-west direction because of the filtering described earlier. The disadvantage of the EOF analysis is the smoothing in time and space to obtain uniform data coverage. This results in the loss of detail in the areas with good coverage. The original 2° latitude resolution, which is desirable for computing north-south derivatives (Wyrtki and Meyers, 1975a), is reduced to 4° in the EOF analysis. However, the method of filling in the data void areas used by Barnett probably obtains more consistent results than the subjective techniques. Another method for filling in the data void regions for the MSC analysis would be to make use of least-squares fitting of low-order spherical harmonics for a first guess field (J.J. Stephens, 1979, personal communication).

The present subjective data set is the only one at this time on a 2° x 2° grid. It is doubtful that either of the objective approaches discussed above, or even a more sophisticated MSC routine, would greatly change the spectral analysis of this paper, with the exception of a slight reduction in the noise level.

3. REVIEW OF SPECTRAL TECHNIQUES

This section will review the basic spectral techniques that are employed on the data set. The data allows a detailed look at the horizontal distributions of the frequency and wavenumber spectra of the wind stress field over the tropical Pacific Ocean. Statistically, the data set is very limited, allowing for only 120 points in time (ten years) and 60-80 equally spaced points in space (i.e., in a latitudinal band). However, this still allows for certain conclusions to be made with reasonable confidence.

a. Direct Fourier transform (DFT) method

Consider a series, τ, consisting of N equally spaced elements, τ_k, k = 1(1)N,

$$\tau_k = \tau(k\Delta), \tag{3}$$

where Δ is the sampling interval (in time or space), such that

$$T = N\Delta, \tag{4}$$

where T is the series length. τ_k can be represented by the Fourier transform pair

$$\tau_k = \sum_{m=-n}^{n-1} c_m \exp(-i2\pi mk/N)$$

$$c_m = \frac{1}{N} \sum_{k=1}^{N} \tau_k \exp(i2\pi mk/N), \tag{5}$$

$$c_m = \frac{1}{N} \sum_{k=1}^{N} \tau_k \exp(i2\pi mk/N), \tag{5}$$

where c_m are complex Fourier coefficients, and n = N/2. The sample mean is then given by c_0, i.e.,

$$c_0 = \bar{\tau} = \frac{1}{N} \sum_{k=1}^{n} \tau_k. \tag{6}$$

Thus, using (5), the sample variance, given by

$$s^2 = \frac{1}{N} \sum_{k=1}^{N} (\tau_k - \bar{\tau})^2, \tag{7}$$

can also be expressed as

$$s^2 = \sum_{m=-n}^{-1} |c_m|^2 + \sum_{m=1}^{n-1} |c_m|^2. \tag{8}$$

If the series τ_k is real, it can be shown that

$$c_m = c^*_{-m} . \tag{9}$$

Then, (5) can also be written as

$$\tau_k = c_0 + 2 \sum_{m=1}^{n-1} c_m \exp(-i2\pi mk/N) + c_n \cos(\pi k). \tag{10}$$

The variance, s^2, is given more simply by

$$s^2 = 2 \sum_{m=1}^{n-1} |c_m|^2 + |c_n|^2. \tag{11}$$

This means that the squared modulus of the complex transform of the data partitions the sample variance into frequency/wavenumber space. The sample raw spectrum is then defined as:

$$S_m = \begin{cases} 2T\,|c_m|^2, & m = 1(1)n-1 \\ T\,|c_m|^2, & m = 0,\ n. \end{cases} \tag{12}$$

$$S_m = \begin{cases} 2T\,|c_m|^2, & m = 1(1)n-1 \\ T\,|c_m|^2, & m = 0,\ n. \end{cases} \tag{12}$$

Then, for the spectral estimates, S_m,

$$s^2 = \frac{1}{T} \sum_{m=1}^{n} S_m = \frac{1}{N\Delta} \sum_{m=1}^{n} S_m. \tag{13}$$

The fundamental frequency/wavenumber, and thus the increment of frequency/wavenumber, is given by

$$\Delta f = 1/N\Delta. \tag{14}$$

Therefore, the area under a plot of S_m versus frequency/wavenumber is equal to the sample variance.

When more detail is desired in the lower harmonics, the frequency/wavenumber is plotted on a logarithmic scale. If the ordinate is given as $S_m f_m$, where f_m is the frequency of the m^{th} harmonic, then the area under the plot is once again equal to the sample variance, because:

$$\begin{aligned} f_m &= m\Delta f = m/N\Delta \\ \sum_m [S_m f_m \Delta ln(f_m)] &= \sum_m S_m \Delta f. \end{aligned} \tag{15}$$

For this study, smoothing is applied to the spectral estimates by the use of Hanning passes. Each of these passes is a weighted running average with weights ($\frac{1}{4}$, $\frac{1}{2}$, $\frac{1}{4}$). The smoothed estimates, $\overline{S}_m$, for one Hanning pass are defined by

$$\overline{S}_m = \frac{1}{4} S_{m-1} + \frac{1}{2} S_m + \frac{1}{4} S_{m+1}. \tag{16}$$

b. Degrees of freedom

The standard methods for calculating the degrees of freedom, bandwidths and 80 percent confidence limits are given in Jenkins and Watts (1969). It is desirable for the degrees of freedom to be high in order to increase the stability of the spectral estimates. The record lengths (4) for this study are very short. A large number of Hanning passes, which would create the desired degrees of freedom, would also greatly decrease resolution of the smaller details of the spectra.

Instead, an alternate method is used to increase the degrees of freedom. For the complete frequency spectra, which will be presented in Section 4b, the spectral estimates are averaged for 11 adjacent points in the longitudinal direction after Hanning. However, because the original data were averaged for 10° longitude bands and the subjective data set is at 2° intervals, each neighboring point cannot be regarded as statistically independent. Upper and lower limits for the degrees of freedom were calculated, along with their respective confidence limits. Let the degrees of freedom for the spectral estimates at each point after the Hanning passes be given by ν_H. The upper bound for the degrees of freedom, ν_H, is based on the assumption that all of the neighboring data points are mutually independent. The lower bound, ν_L, is based on the conservative assumption that the 10° bands are mutually independent. The upper and lower bounds for p adjacent points, each with degrees of freedom, ν_H, are given by

$$\nu_L = (\mathrm{INT}[p/6] + 1)\nu_H$$

$$\nu = p\nu_H \qquad (17)$$

$$\nu_L = (\mathrm{INT}[p/6] + 1)\nu_H$$

$$\nu_U = p\nu_H, \qquad (17)$$

where INT[ ] gives the integer part of the quantity in the brackets. Two Hanning passes are performed on the averaged frequency spectra before plotting. According to (17), ν_U and ν_L the upper and lower bounds of the degrees of freedom, are equal to 80.5 and 14.6, respectively.

Ten-year averages are calculated for the wavenumber spectra distributions for January, February, etc. Each of the years are mutually independent. The degrees of freedom is given by ν_U in (17), with p now equal to the number of years used for the averages. Three Hanning passes are performed on the averaged spectra before plotting. For this case, the degrees of freedom is equal to 88.7.

c. Spectral analysis procedure

This section gives the procedures that are used to obtain the frequency spectra and the seasonal wavenumber spectra for the subjectively analyzed data. A similar analysis is done for τ, τ_x and τ_y separately, for the frequency spectra. The wavenumber spectra are only computed for τ, the magnitude of the wind stress.

The procedure used in this study for the frequency spectra of the stress data is as follows (performed for the time series at each point in space):

1. The mean, and in some cases linear trend, are removed.
2. A DFT is performed using the subroutine FOURT.
3. The raw spectral estimates, S_m, and the sample variance are computed according to Eq. (12) and (13). In some cases, these are averaged over a longitude band.

computed according to Eq. (12) and (13). In some cases, these are averaged over a longitude band.

4. The smoothed spectral estimates, $\overline{S}_m$, are obtained using up to two Hanning passes.

The procedure to obtain the wavenumber spectra is identical to the above procedure with the following exceptions:

1. After the linear trend is removed, the series length for each latitude is extended by zeros to 80 points (i.e., 160° longitude).
2. The spectra computed from the extended series, S'_m, are adjusted by the factor N'/N, where N' is the extended series length of 80 points, and N is the initial series length. The final S_m, given by

$$S_m = \frac{N'}{N} S'_m , \tag{18}$$

have the property

$$s^2 = \frac{1}{N'\Delta} \sum_{m=1}^{n'} S_m = \frac{1}{N\Delta} \sum_{m=1}^{n'} S'_m, \tag{19}$$

where n' = N'/2.

3. The spatial spectral estimates are averaged over the ten-year period to produce monthly mean values for January, February, etc. for each latitude band.
4. Three Hanning passes are used to calculate $\overline{S}_m$.

4. FREQUENCY SPECTRA

The characteristics of the bimonthly averages for the period 1947-1972, as well as overall seasonal and annual averages have already been discussed in detail for the original data (Wyrtki and Meyers, 1975a, b, 1976). Barnett (1977a) and Busalacchi (1979, unpublished manuscript) have reviewed the mean distributions for the original and subjectively analyzed data, respectively. It is doubtful that the monthly averages in this data set contain significant differences from the original data set. Therefore, this section will focus its attention on the distributions of the significant parts of the frequency spectra.

General oceanic circulation models depend on linear forcing by the wind stress. Other models, such as those involving the deepening of the mixed layer, are regulated by a power of the magnitude of the wind stress. Therefore, this study will look at the spectra for τ, τ_x and τ_y, separately. In particular, the distributions of the annual, semi-annual and total low frequency variability will be discussed, as well as the distribution of the total variance. Barnett (1977a) has analyzed the original data using empirical orthogonal functions (EOF). Busalacchi (1979, unpublished manuscript) performed the same analysis using the subjective data set. The distribution of energy in the annual cycle, discussed later in this section, agree well with their results for seasonal variability

annual cycle, discussed later in this section, agree well with their results for seasonal variability.

For this study, the variance, s^2, given by (8), was computed for the time series at each point of the 2° by 2° grid. These values are shown for τ, τ_x and τ_y, in Fig. 3. The time series were then analyzed as described in Section 3, for τ, τ_x and τ_y, independently. The plots of the spectral density, $\overline{S}_m$ are shown in Fig. 4-9 for τ, τ_x and τ_y, for selected longitudinal bands (see Fig. 2). The spectral estimates are averaged over bands of eleven points in order to improve statistical stability. The upper and lower limits of the degrees of freedom are calculated according to (17). The smoothed spectral estimates, $\overline{S}_m$, for the annual signal are plotted in Fig. 10. The semiannual distributions are shown in Fig. 11.

There is a great deal of interest in the interannual variability of the wind stress. The long term changes are believed to be related to the anomalous heavy rainfall over the central and western equatorial Pacific (Quinn and Burt, 1970, 1972) as well as to El Niño invasions (Bjerknes, 1966; Quinn, 1974; Wyrtki, 1975; Kindle, 1979; O'Brien et al., 1979). The short record length in this study does not permit sufficient resolution of the interannual peaks (if they exist). Instead, the distribution of the total energy for the signals with periods greater than or equal to 20 months is plotted for τ, τ_x and τ_y (Fig. 12). The energy for the periods between 12 and 20 months is not used in order to eliminate leakage from the strong annual signal. Because of excessive noise in the patterns, and to make the principal features more visible, the patterns are smoothed by hand. Two degrees of shading are used rather than contours. A linear trend in the data is often the

visible, the patterns are smoothed by hand. Two degrees of shading are used rather than contours. A linear trend in the data is often the result of leakage from signals with frequencies lower than the fundamen-

tal frequency (14). Therefore, the linear trends are not removed for this section, so that all of the interannual variability would be included. The whiteness of the spectra in the low frequencies will be discussed further in Section 6.

The reader should recall from Section 2 that the original data were very sparse in some areas (see Fig. 1). In particular, one should be cautious in drawing conclusions concerning the two large areas of poor data coverage which lie near the dateline from about 5°N-10°S, and to the west of Chile from 15-29°S.

a. Distribution of total variance

All three charts contain a band of high variance lying between the core regions of the northeast and southeast trades, roughly from 5-15°N. The band for τ_y lies the farthest south, and coincides with the average position for the ITCZ in the eastern half of the basin. The bands in τ and τ_x lie slightly farther to the north, stretching almost continuously to the maxima in the northwestern part of the basin, whereas τ_y exhibits very low variance from about 150°W to 150°E.

There are high variance areas on the northern and southern borders showing up primarily in τ_x, but also slightly in τ. These are due to the intrusion of the winter mid-latitude storm-tracks into the subtropics. This feature is not present in the τ_y chart. When monthly averages are used, the meridional component of the mid-latitude cyclones will tend to cancel itself, whereas the zonal component will not.

The other major features of the distribution of variance are located will tend to cancel itself, whereas the zonal component will not.

The other major features of the distribution of variance are located in the northwest and southwest portions of the basin. These are related

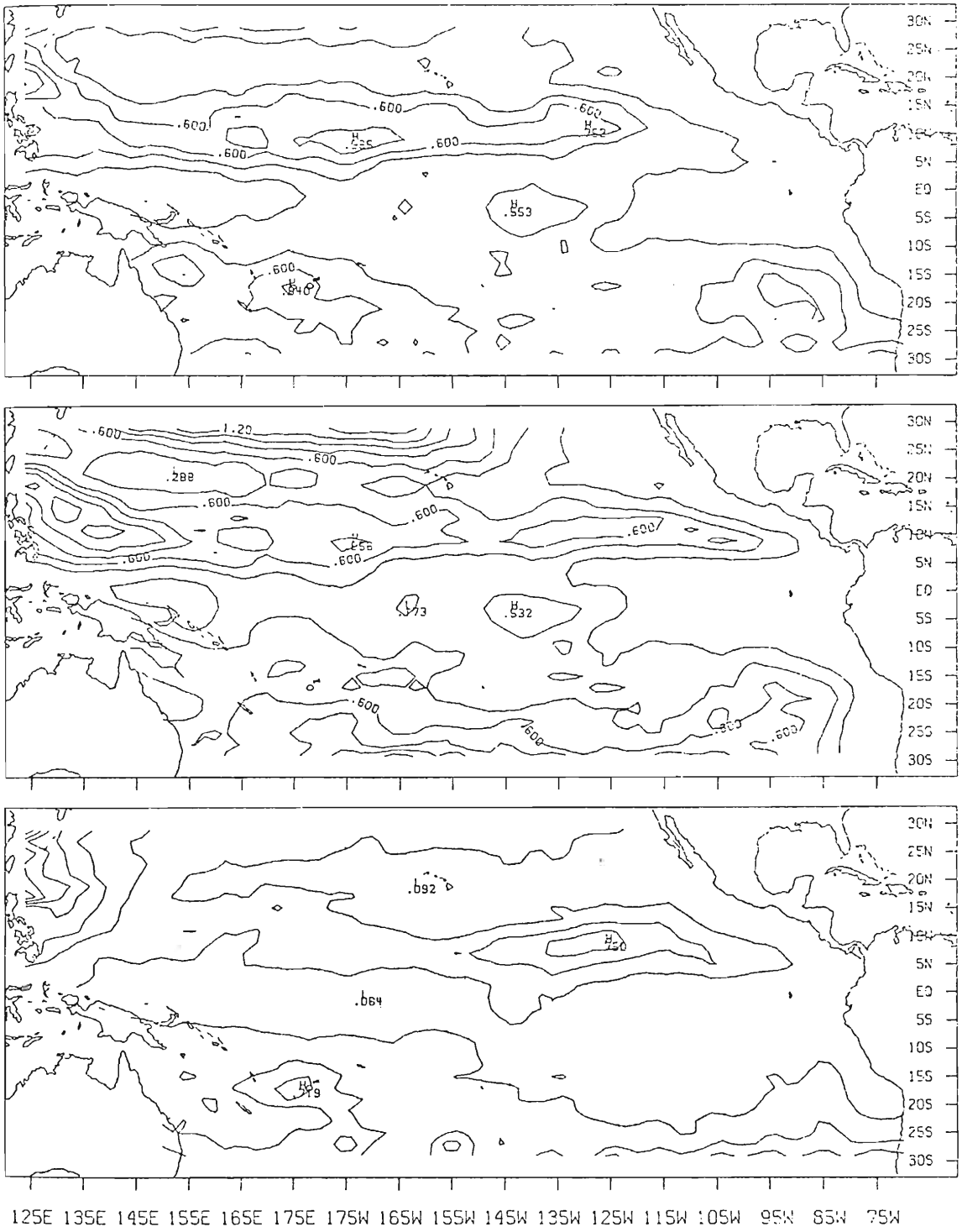

Fig. 3. Spatial distribution of the total variance of the time series for (a) τ, (b) τ_x and (c) τ_y. The linear trends were not removed from the series prior to computing the variances. The contour interval is .2 m^4 s^{-4} x 10^3.

Fig. 3. Spatial distribution of the total variance of the time series for (a) τ, (b) τ_x and (c) τ_y. The linear trends were not removed from the series prior to computing the variances. The contour interval is .2 m^4 s^{-4} x 10^3.

to the monsoon circulations of southeast Asia and northeast Australia, respectively. Although the total variance of τ_x is not high in the latter region, it still exhibits a strong annual signal which will be discussed later.

As expected, all three fields show relatively low variance along the equator. Also, with the exception of the narrow band of high variance in τ_x, the easternmost portion of the basin north of 21°S has very low total variance.

Also of interest is the area of high variance to the southwest of Peru, primarily in the τ and τ_x fields. This feature could be attributed to the variations in the southeast trades north of the center of the subtropical high. However, this is in a region of poor data coverage, so much of the variance there might be due to noise.

b. Examples of complete spectra

The most outstanding feature of the spectra is the prominent annual peak appearing in Figs. 4, 5 and 6. The only other statistically significant peak is the semiannual signal in some of the plots. Excluding the annual and semiannual, the spectra are essentially "white" (i.e., flat). These features, and their differences for plots of the spectra of τ, τ_x and τ_y, will be discussed briefly for the six plots. The conservative lower limit of the degrees of freedom will be used in interpreting these plots.

In an analysis of the quasi-geostrophic wind field over the northern Atlantic and Pacific Oceans, Willebrand (1978) found the frequency spec-

In an analysis of the quasi-geostrophic wind field over the northern Atlantic and Pacific Oceans, Willebrand (1978) found the frequency spec-

tra to be essentially white for periods greater than 10 days. For wind

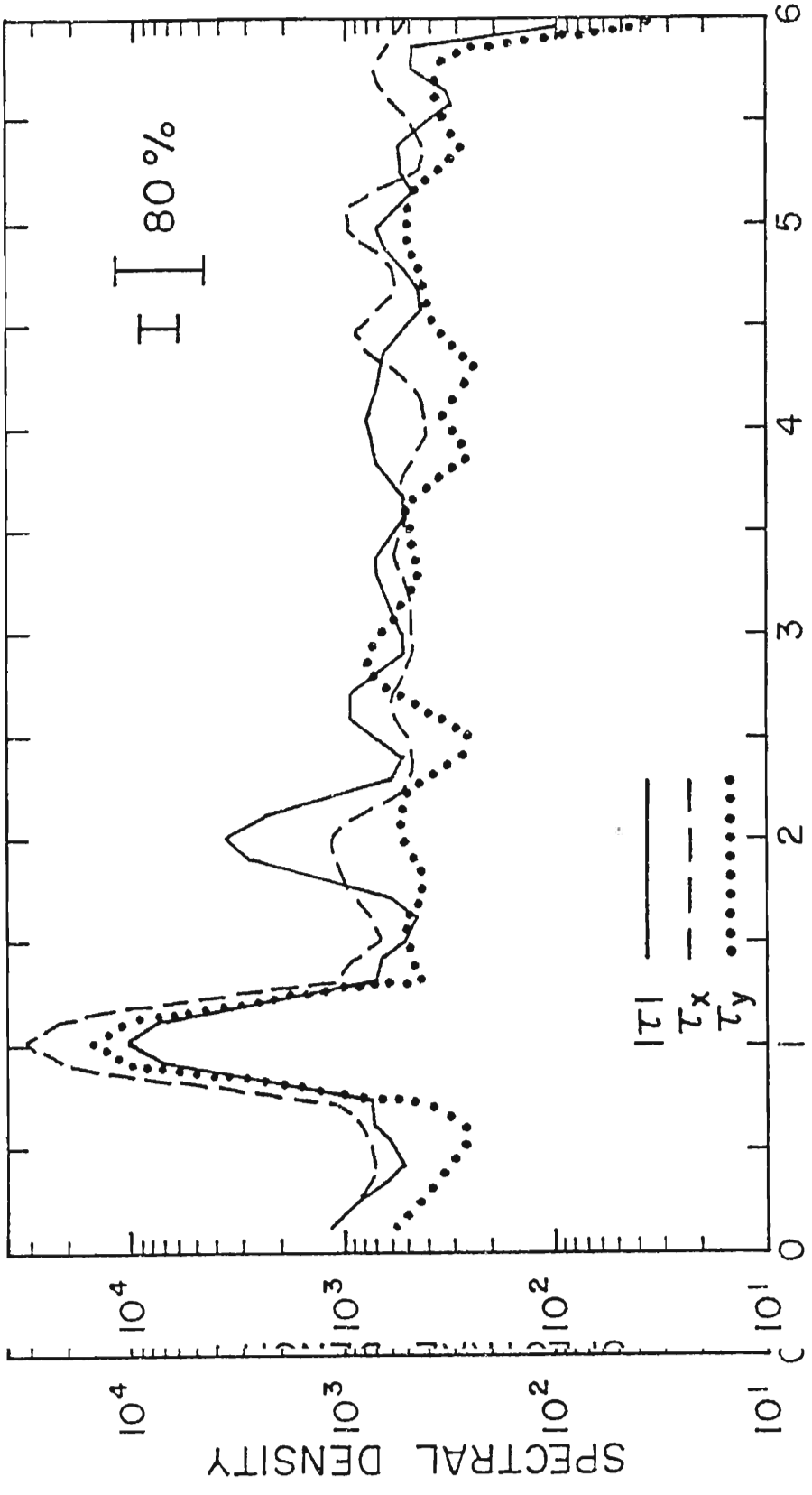

Fig. 4. Power spectra for τ, τ_x and τ_y for 11°N, 124-144°E. Units for the spectral density are ($m^4 s^{-4}$)(months). The raw spectra, S_m^{XY}, were smoothed by two Hanning passes. The smaller and larger 80 percent confidence limits correspond to the upper and lower bounds on calcon calculating ν (see (17)).

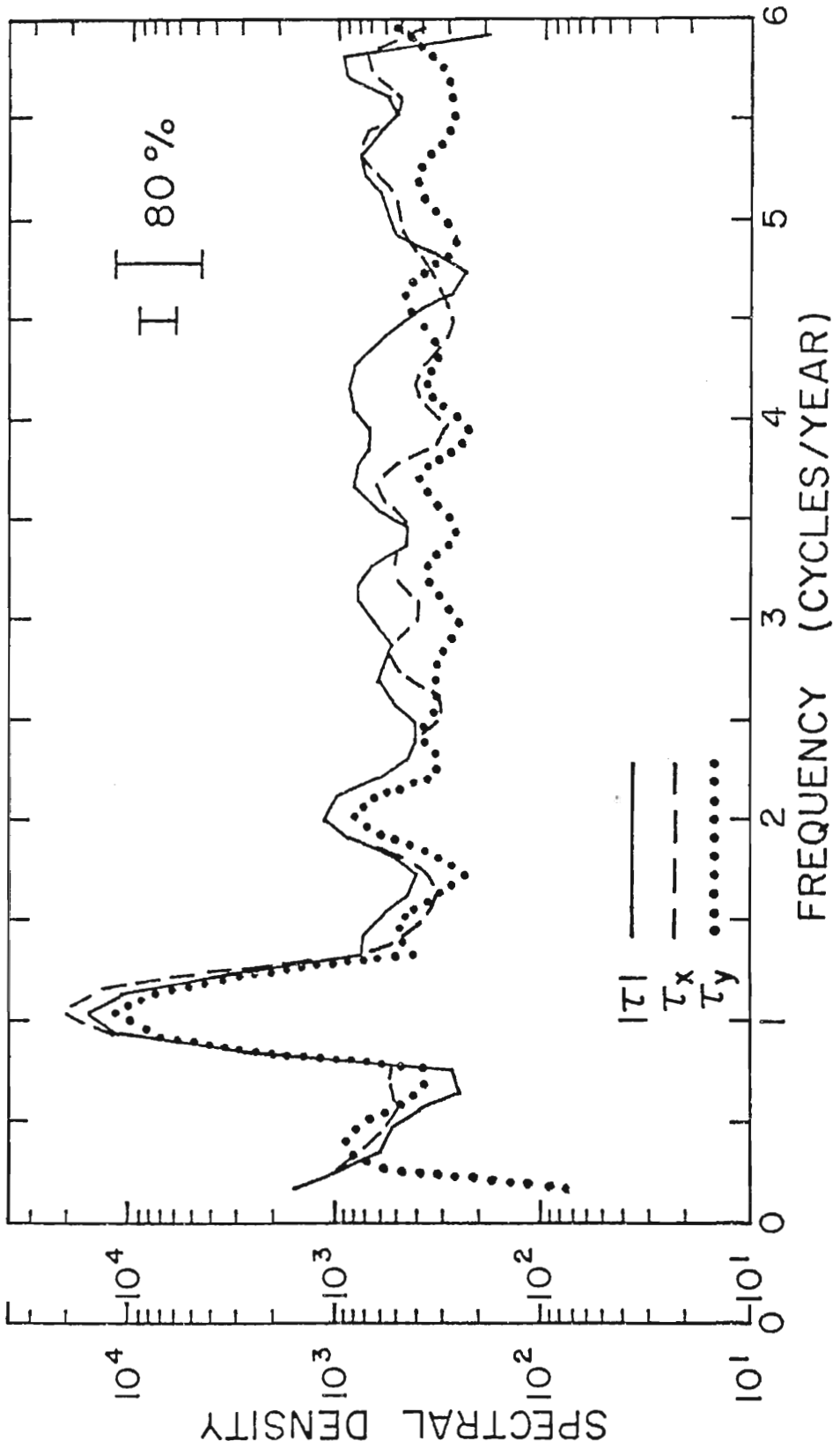

Fig. 5. Same as Fig. 4, except for 11°N, 122-142°W.

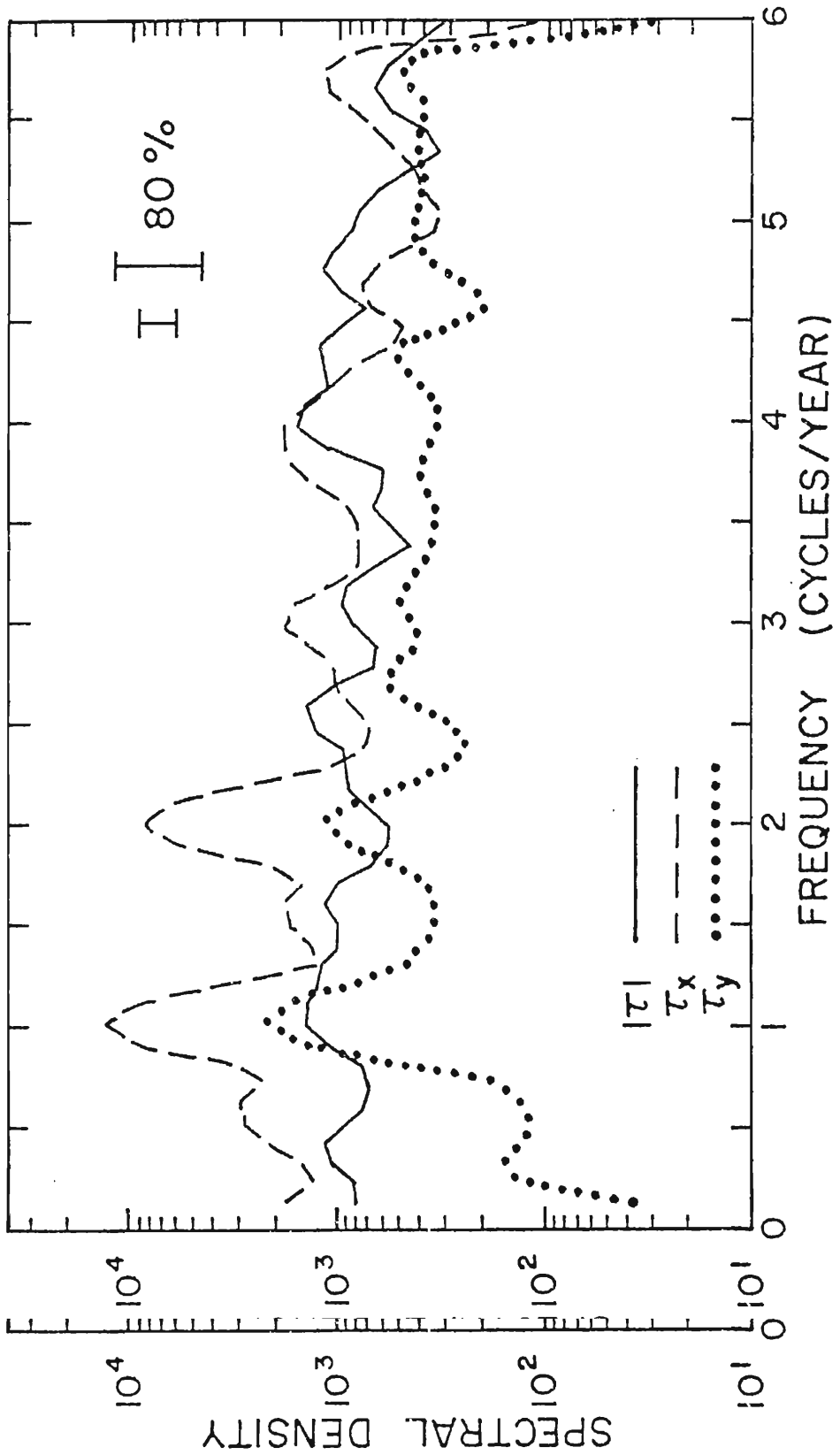

Fig. 6. Same as Fig. 4, except for 27°N, 164°E-176°W.

data at 52.5°N, 35.5°W, he found the annual signal more pronounced in the spectrum of the stress magnitude than in the spectra for the stress components. This study shows that the relative power of the annual signal in τ, τ_x and τ_y can vary greatly from region to region.

1) 11°N, 124-144°E (Fig. 4)

This longitudinal band lies in the region dominated by the southeast Asian monsoon. The annual peak is strongest in the spectrum of τ_x, followed closely by the annual peak in τ_y and τ. There is a significant semiannual peak in the τ spectrum, while no well formed semiannual peak appears in the spectra for τ_x or τ_y. This feature will be discussed further under annual variability. The rest of the spectra are essentially flat.

2) 11°N, 122-142°W (Fig. 5)

This region is located near the mean position for the ITCZ in the eastern section of the basin. The prominent annual peak is strongest in the τ_x spectrum, but it is not significantly different from that for τ or τ_y. The remainder of the spectra are white, except for a small semiannual peak. The spectra for τ and τ_x show signs of leakage due to power from very low frequencies (below .1 cpy). The low frequency energy in τ_y is concentrated around a period of about 3.3 years (although the peak is not statistically significant).

3) 24°N, 164°E-176°W (Fig. 6)

This band lies in the region of the basin affected by the intrusion of winter mid-latitude storm tracks. It is strikingly different from the previous two plots due to the flatness of the stress magnitude spec-

of winter mid-latitude storm tracks. It is strikingly different from the previous two plots due to the flatness of the stress magnitude spec-

trum, even though there are pronounced peaks in the spectra for both of

the components. The spectra for τ_x and τ_y exhibit significant annual and semiannual peaks. The τ_y spectrum shows a noticeable absence of interannual variability, which is very high for τ_x and moderate for τ. One additional feature is that the τ_x spectrum is red, although the slope is not very steep. This feature is also present to a lesser extent in the τ_x spectrum for 27°S, 156-176°W (not shown), which corresponds to the intrusion of winter storm tracks into the Southern Hemisphere subtropics. The redness of the τ_x spectra in these two cases suggests that this feature is associated in some way with the seasonal variation of mid-latitude cyclone tracks.

4) 23°S, 174°E-166°W (Fig. 7)

All three of the spectra for this region, which is located in the southwest Pacific, are white. Although there are slight annual peaks in the τ, τ_x and τ_y spectra, they are not significant relative to the 80 percent confidence interval. There is a relatively large amount of energy in the interannual band, particularly for the τ and τ_x spectra. Barnett (1977a) found that the maximum interannual variations in the trades occur primarily in the west and southwest Pacific. The distribution of low frequency energy will be discussed later in this section.

5) 3°S, 178°E-162°W (Fig. 8)

This band is centered on Canton Island in the equatorial Pacific. The spectra for both τ and τ_x are flat. The τ_y spectrum contains a significant annual peak. The low frequency variability in τ and τ_x is concentrated around a period of about 2.2 to 2.5 years.

concentrated around a period of about 2.2 to 2.5 years.

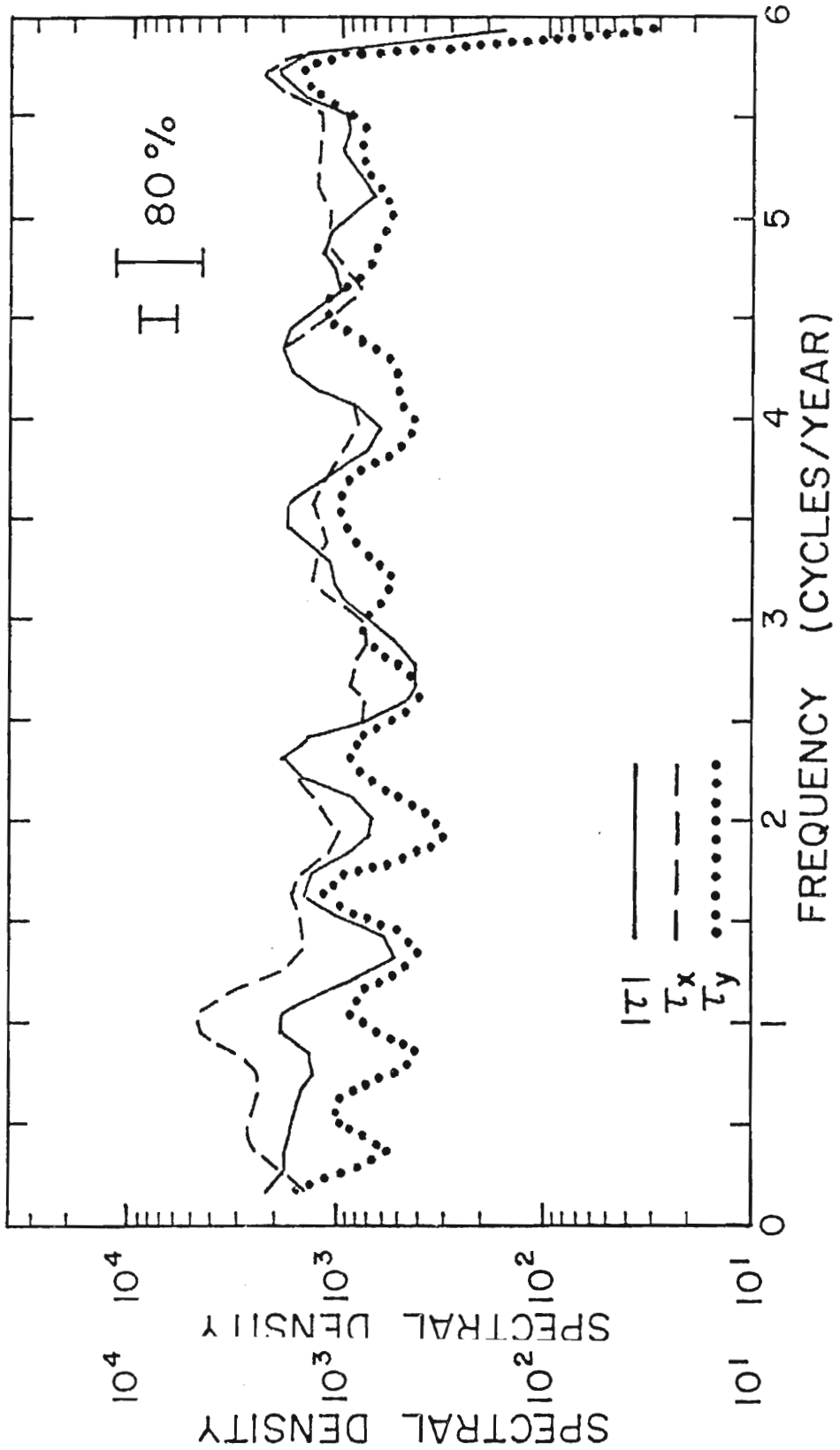

Fig. 7. Same as Fig. 4, except for 23°S, 174°E-166°W.

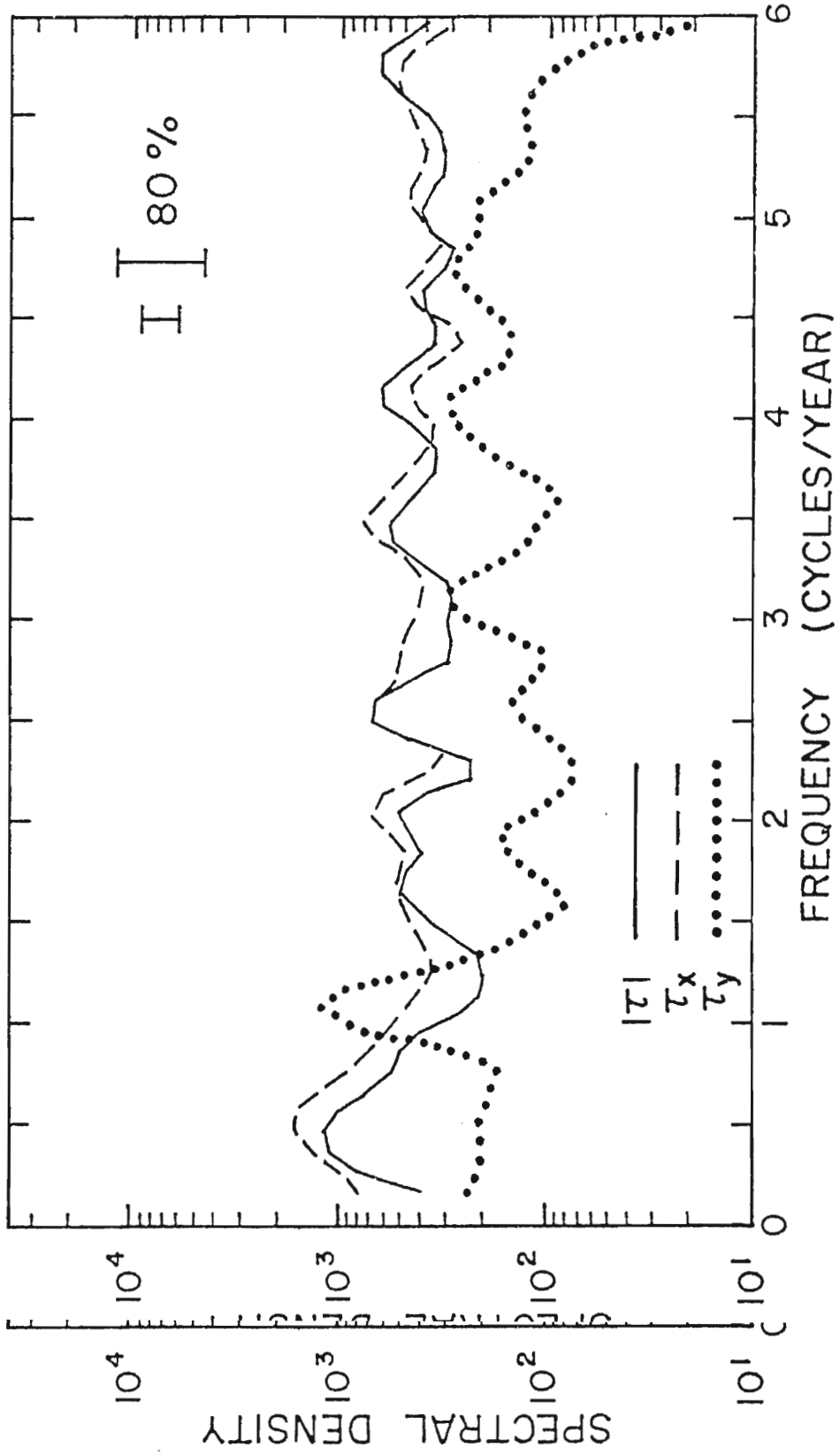

Fig. 8. Same as Fig. 4, except for 3°S, 178°E-162°W.

6) 17°S, 84-104°W (Fig. 9)

The spectra for this region, which lies just north of the Southern Hemisphere subtropical high, contain no significant annual signal. There is a slight semiannual peak in the spectra for τ and τ_x, but it is not statistically significant. It is possible that the lack of a significant resolved peak for this band is related to the poor data coverage in this area.

c. Distribution of annual variability

It is apparent from the spectra discussed above that the highest variability is in the annual cycle. It is not surprising therefore, that the distribution of the annual signal is similar to that for the total variance. As was the case for the complete spectra, there are distinct differences in the distribution of the annual signal between the stress magnitude and its two components.

The plots for τ, τ_x and τ_y all display a band of very high annual energy lying approximately along the mean position of the ITCZ to the east of the dateline. The maximum for this area in the annual signal for τ_y is located along 9°N, while the eastern maxima for τ and τ_x are both at 11°N. The very high values for the annual signal in τ and τ_x extend across the basin to the west, while the high values in τ_y drop off markedly from about 155°W westward to about 145°E. These differences lead to the conclusion that this area of high annual variability in τ_y is associated primarily with the seasonal variation of the position of the ITCZ, whose position fluctuates the most in the eastern Pacific (Atkinson, 1971). The high annual signal in τ and τ_x in this region is associated with the seasonal oscillation in the strength of

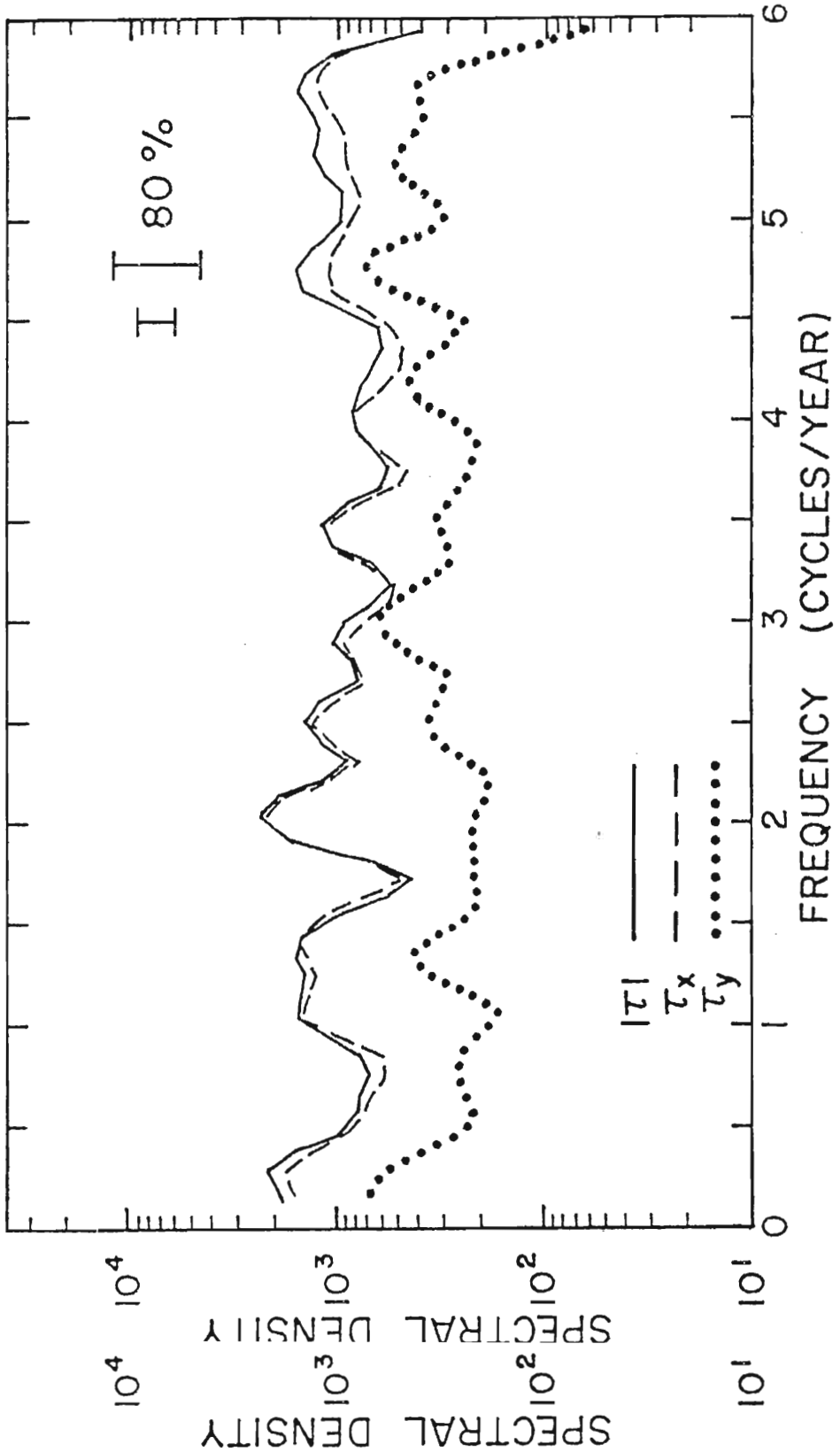

Fi Fig. 9. Same as Fig. 4, except for 17°S, 84-104°W.

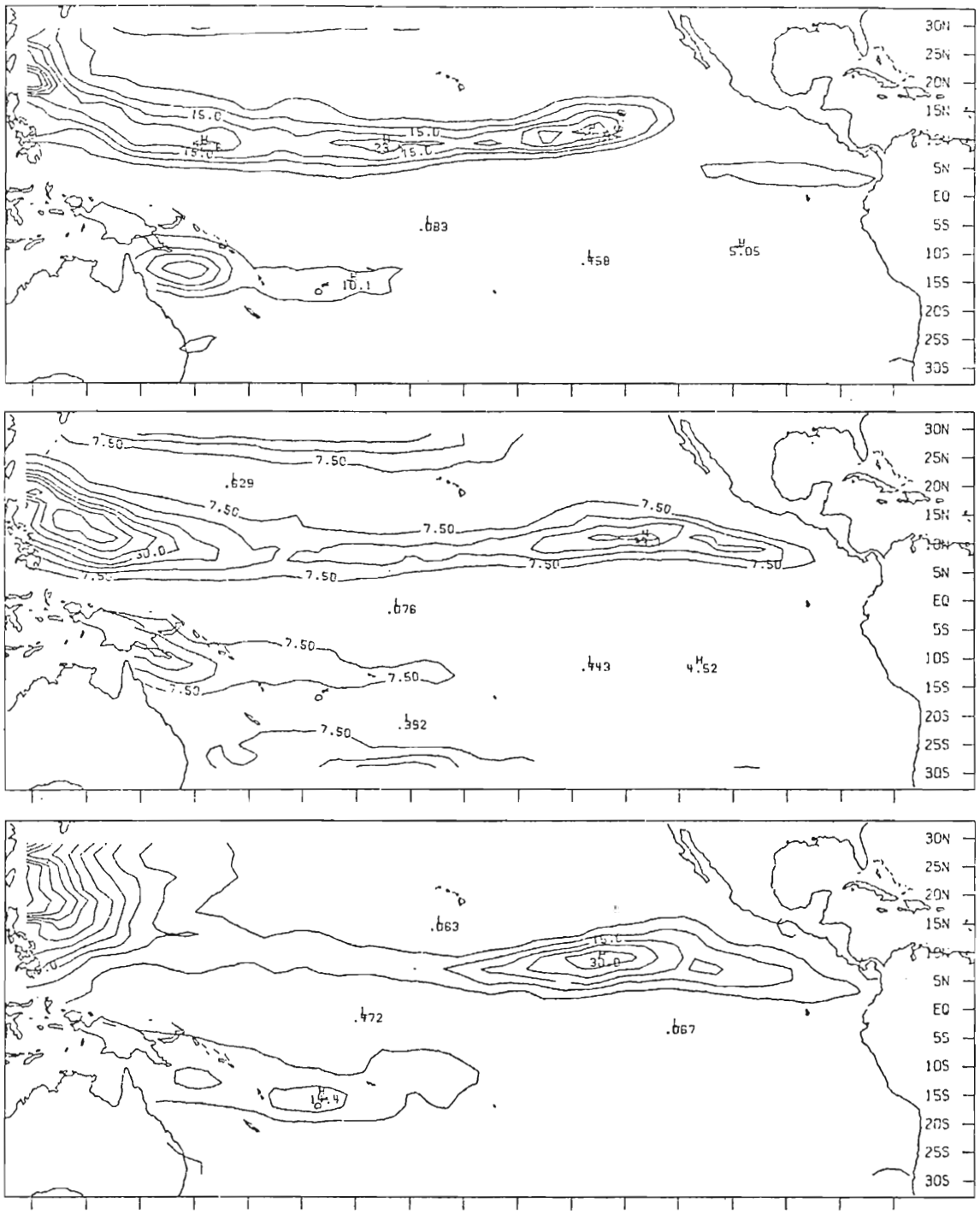

Fig. 10. Spatial distribution of the power in the annual signal for (a) τ, (b) τ_x and (c) τ_y. One Hanning pass was performed on the raw spectral estimates before plotting. The contour interval for (a) and (c) is 5$(m^4\ s^{-4})$(months) x 10^3 and for (b) is 7.5 $(m\ s^{-4})$(months) x 10^3.

(a) τ, (b) τ_x and (c) τ_y. One Hanning pass was performed on the raw spectral estimates before plotting. The contour interval for (a) and (c) is 5$(m^4\ s^{-4})$(months) x 10^3 and for (b) is 7.5 $(m\ s^{-4})$(months) x 10^3.

the northeast trades. Wyrtki and Meyers (1976) demonstrated that the annual variations in the area and strength of the northeast trades are larger than that for the southeast trades.

The plots for τ, τ_x and τ_y all contain an area of high annual variability in the northwestern corner of the basin. This feature, a product of the monsoon circulation of southeast Asia, was discussed in the previous part of this section for Fig. 4. This is an excellent example of a case in which the annual signal is larger for the components than for the stress magnitude. Because of the winter and summer monsoons, the mean flow at 11°N, 125°E, is from the northeast, November through April, and from the southwest, July through October (Wyrtki and Meyers, 1975a). This results in a large annual variation in the wind components. The reader may want to convince himself, that although the wind components exhibit a strong annual signal, some of this annual variability might show up as a strong semiannual signal in the spectrum of the wind speed. Such is the case demonstrated in Fig. 4. The spectra for τ_x and τ_y both contain a large annual peak, but no semiannual peak. The spectrum for τ displays a smaller annual peak, but also a pronounced semiannual peak. This is an important consideration for looking at the oceanic response to the winds. The deepening of the mixed layer in the ocean responds to the magnitude of the wind stress. Therefore, in some cases, a portion of the annual variability in the wind field can show up as semiannual variability in the depth of the mixed layer.

The maxima off northeast Australia are consequences of the mixed layer.

The maxima off northeast Australia are consequences of the Australian monsoon. The areas of high power for the annual signal in τ_x

(and showing up slightly in τ) in the extreme north and south of the basin are the result of the intrusion of mid-latitude winter cyclones into the Northern and Southern Hemisphere, respectively. Both of these features have been discussed previously in this section with respect to the distribution of total variance.

The time amplitude functions for the U2 and V2 eigenvectors of the EOF analysis performed by Barnett (1977a) and Busalacchi (1979, unpublished manuscript) are modulated seasonal signals. The eigenvector patterns and the major features of the distribution of the annual variability in this study are very similar. The differences are probably due to the coarser spatial resolution employed in the EOF analyses. Also, Barnett's analysis covered a longer timespan, 1950-1972, than the subjectively analyzed data.

d. Distribution of semiannual variability

There are five areas displaying high semiannual energy. The semiannual variability of the region which lies off the Phillipines, and the region to the west of Peru have both been discussed earlier in this section.

The most prominent feature is the region of very high semiannual energy in Fig. 11 to the north of 23°N in the western half of the basin. The complete spectra and the high annual signal have been analyzed previously in this section. The spectra showed a significant semiannual peak, plus small peaks at 3 and 4 cpy (see Fig. 6). The monthly average values for τ_x are very high in winter, yielding a non-sinusoidal annual variation. This results in the "ringing" of the harmonics of age values for τ_x are very high in winter, yielding a non-sinusoidal annual variation. This results in the "ringing" of the harmonics of the annual frequency.

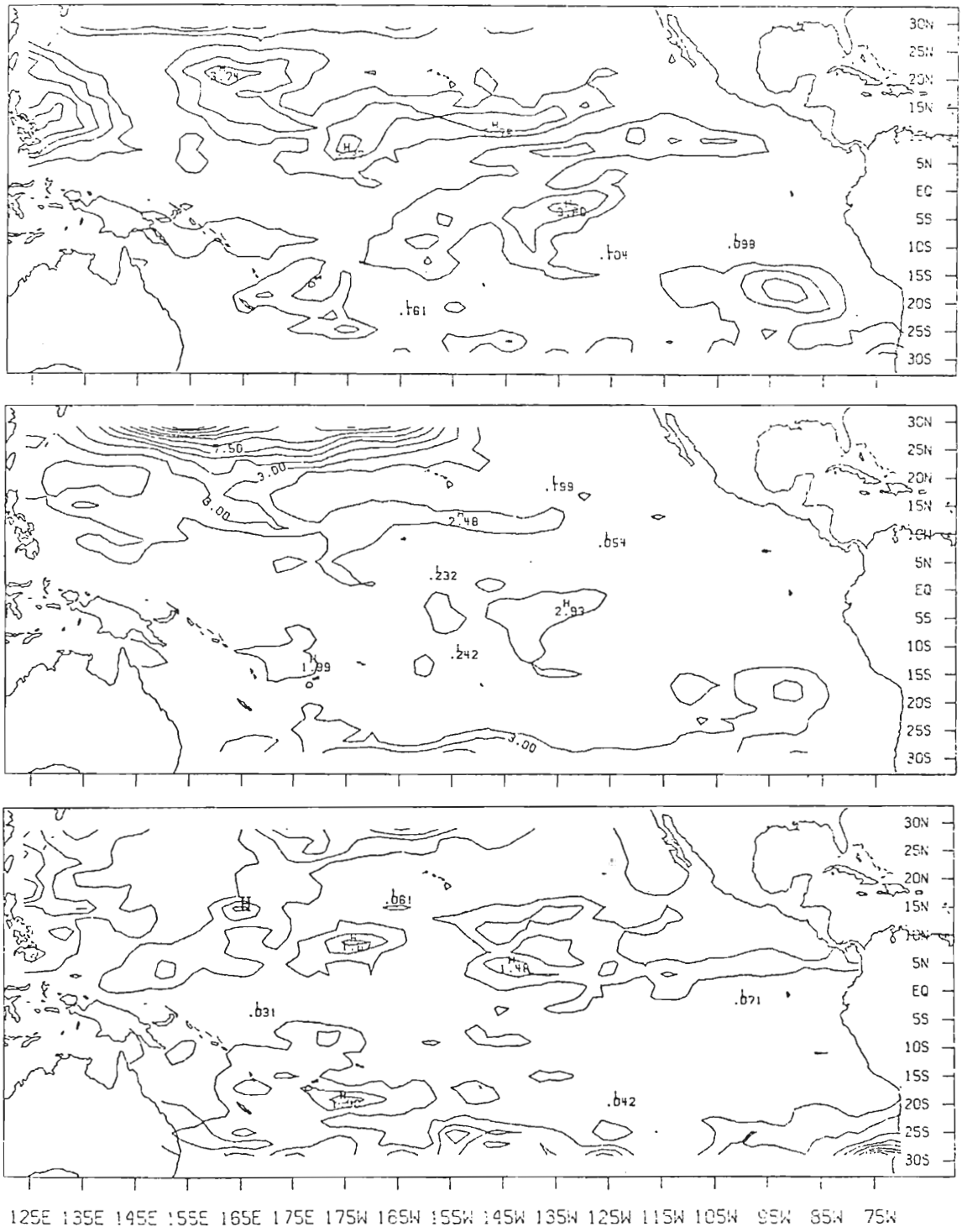

Fig. 11. Spatial distribution of the power in the semiannual (six month) signal for (a) τ, (b) τ_x and (c) τ_y. Two Hanning passes were performed on the raw spectral estimates prior to plotting. The contour

Fig. 11. Spatial distribution of the power in the semiannual (six month) signal for (a) τ, (b) τ_x and (c) τ_y. Two Hanning passes were performed on the raw spectral estimates prior to plotting. The contour interval is 1$(m^4\ s^{-4})$(months) x 10^3 for (a), 1.5 $(m^4\ s^{-4})$(months) x 10^3 for (b) and .5 $(m^4\ s^{-4})$(months) x 10^3 for (c).

The region of high semiannual energy in τ centered at 21°N, 162°E, is a feature resulting from true six-month variability. The seasonal shifting of the subtropical high causes the belt of strongest trades at 162°E to cross this latitude twice annually. This results in maxima for τ and τ_x to occur around April and October (Wyrtki and Meyers, 1975a). The spectra for the band at 21°N, 154-174°E (not shown), contain a significant semiannual peak in τ and τ_x. There is no statistically significant six-month peak for τ_y. (The spectrum for τ_y displays a pronounced annual peak because as the subtropical high moves north, the flow becomes southeast. This produces a large yearly fluctuation about zero.)

The τ_y spectrum (not shown) for the area in the southeast corner of the basin does not exhibit a significant semiannual peak. The relatively high energy there in the semiannual signal could be a product of increased noise due to poor data coverage and extrapolation. This would be in agreement with the study by Hsu and Wallace (1976), which shows a minimum in semiannual pressure variation for that region.

e. Distribution of interannual variability

The most interesting feature is the band of high energy stretching almost continuously across the basin from Chile to Australia. It appears in the distributions for τ, τ_x and τ_y, and is strongest to the west of 120°W. The Southern Oscillation index, the difference in sea level atmospheric pressure between Easter Island and Darwin, Australia, has been used as a method for predicting anomalous equatorial Pacific events such as occurrences of El Niño invasions (Quinn, 1974; Wyrtki has been used as a method for predicting anomalous equatorial Pacific events such as occurrences of El Niño invasions (Quinn, 1974; Wyrtki et al., 1976). This study confirms the idea that the region exhibits

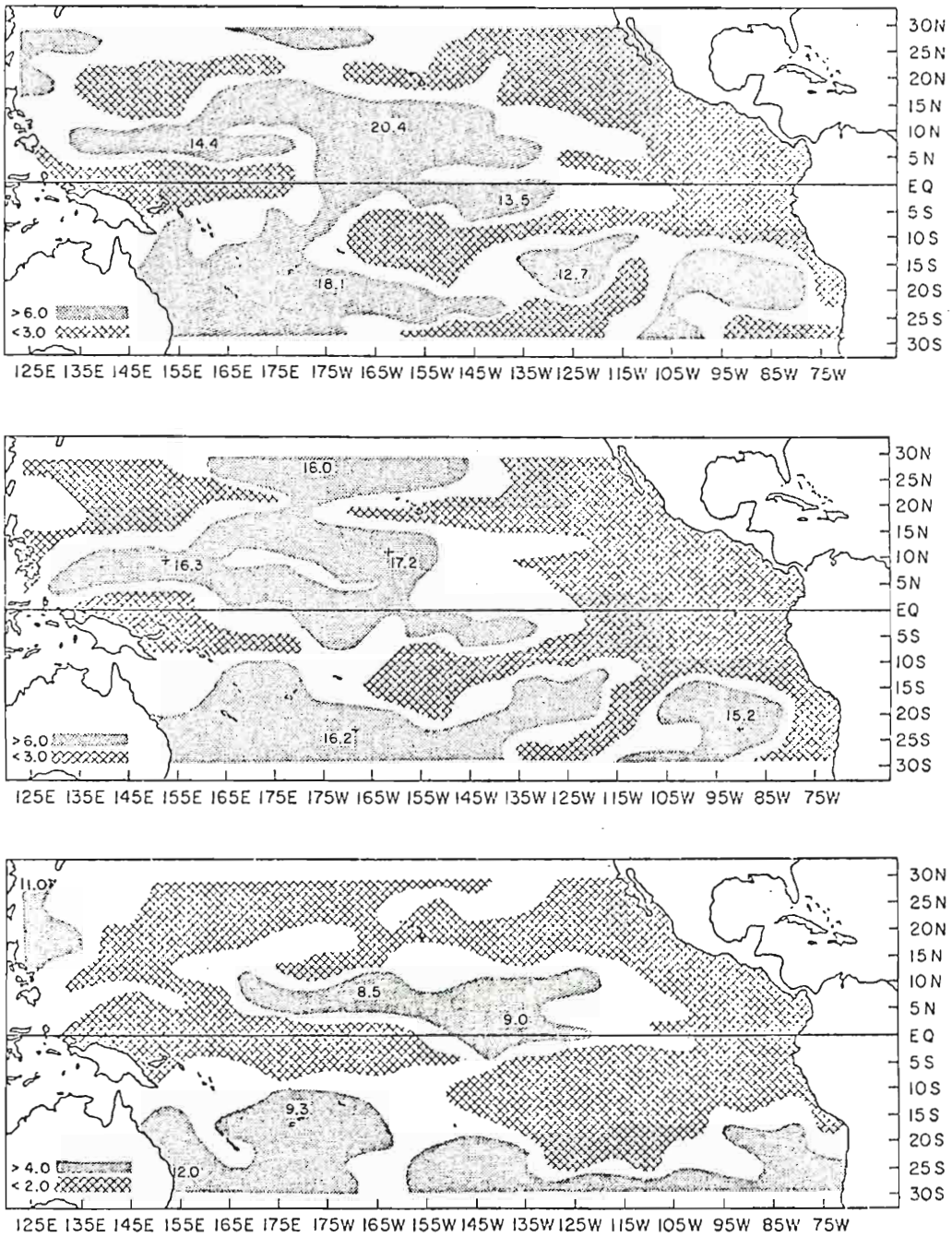

Fig. 12. Distribution of the total low frequency energy for (a) τ, (b) τ_x and (c) τ_y. Some smoothing was done on contours before shading to minimize noise. Values for several selected maxima are given. The units are $(m^4\ s^{-4})$(months) x 10^3.

Fig. 12. Distribution of the total low frequency energy for (a) τ, (b) τ_x and (c) τ_y. Some smoothing was done on contours before shading to minimize noise. Values for several selected maxima are given. The units are $(m^4\ s^{-4})$(months) x 10^3.

high interannual variability.

Another area of high power in the low frequency band lies just north of the equator in the central Pacific for τ, τ_x and τ_y. Wyrtki (1975) previously showed that the central equatorial Pacific exhibits relatively large interannual fluctuations. The high energy areas west of 160°E are in the Asian Monsoon area and may also contribute to El Niño events (O'Brien et al., 1979).

The other area of high energy lies poleward of 21°N in the central Pacific. It is the result of the interannual variability of the degree of southward intrusion and intensity of the middle latitude winter storms.

Of particular importance is the absence of high variability along most of the western coast of North and South America. This is in agreement with the theory that El Niño events are not the result of local wind changes, but are instead caused by remote forcing in the central and western Pacific (Wyrtki, 1975; Barnett, 1977b; Kindle, 1979; O'Brien et al., 1979). The area of high variability in τ, τ_x and τ_y, directly west of Chile, lies in a region of very poor data coverage. The rest of the coast is typified by greater than ten observations per month on the average.

The 12-month running mean of τ_x was plotted for some of the points with very high interannual variability. The long-term oscillations at 23°S, 168°W, and at 29°N, 178°W (not shown), were approximately 180° out of phase. The intensification of the trades for that area (23°S) is accompanied by an increased westerly component at 27°N. The westerlies

accompanied by an increased westerly component at 27°N. The westerlies

at 27°N occur primarily during the winter. Their intensification

is associated with stronger cyclonic circulation from winter storms.

The 12-month running mean of τ_x for 136°W, 3°N, is shown in Fig. 13. This point is located in the southeast trades. The plot is similar to Fig. 4 in Wyrtki (1975), which is for the equatorial band 140-180°W. Based on rainfall records, there were three El Niño events during the period, 1961-1970. Each of the three events took place several months after the magnitude of the zonal component had decreased. This result supports the theory developed by Wyrtki (1975). He stated that, prior to an occurrence of El Niño, there is an increase in the southeast trades over the central equatorial Pacific. This results in a pileup of water in the western half of the Pacific basin. When the trades subsequently relax, the accumulated water will move back towards the east. The water moves east in the form of a downwelling, equatorially trapped Kelvin wave (Hurlburt et al., 1976; McCreary, 1976). It is of special interest that, prior to decreasing in 1963, τ_x was not unusually strong. Thus, a large pileup of water could not have occurred. El Niño at the end of 1963 was in fact weaker than the other two occurrences shown in Fig. 13.

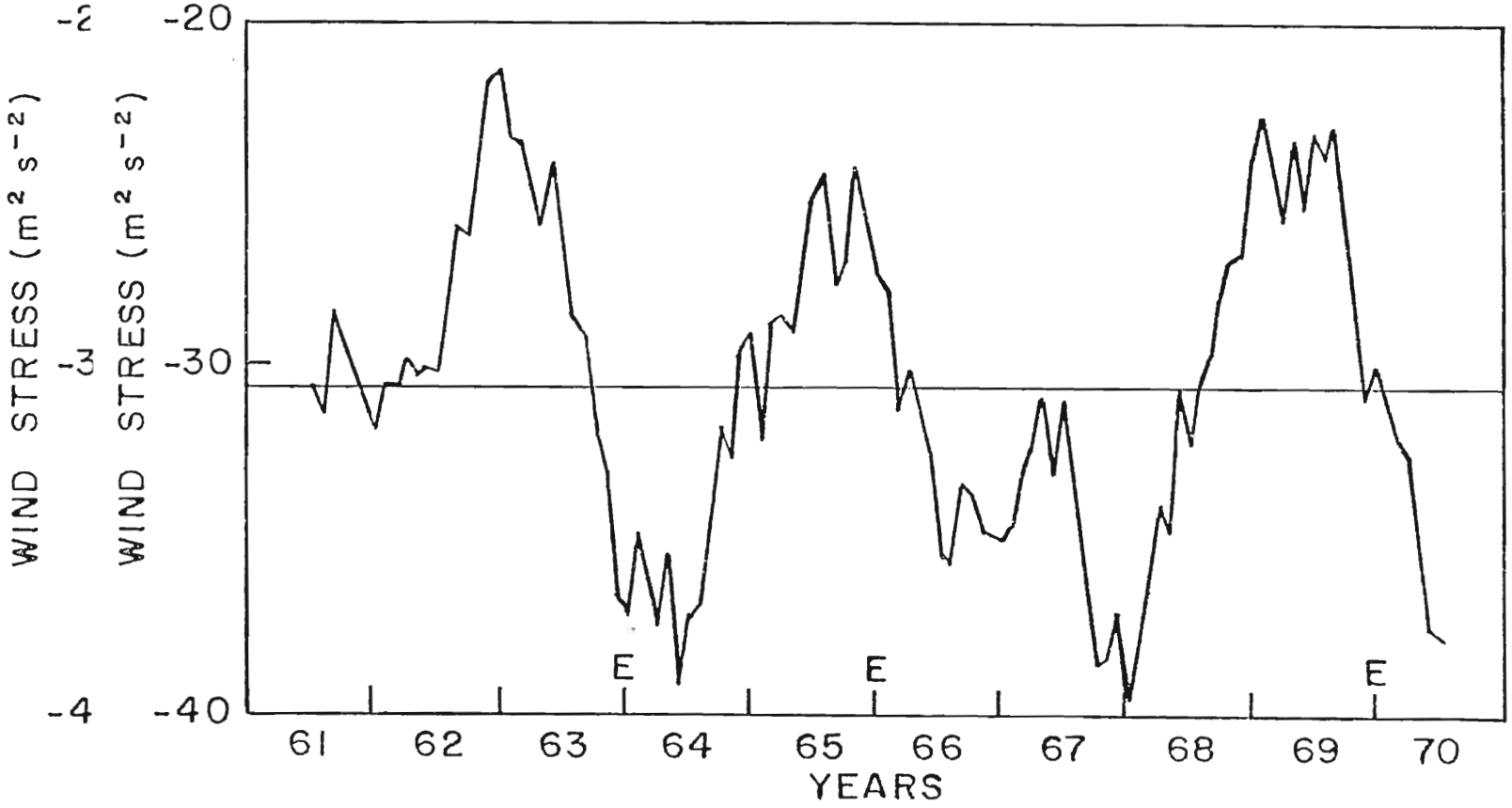

Fig Fig. 13. 12-month running mean for τ_x at 136°W, 3°N. The center solid line indicates the average verage value. Occurences of El Niño are indicated with E's.

5. ZONAL WAVENUMBER SPECTRA

This section will discuss the wavenumber spectra obtained by performing the analysis described at the end of Section 3. T, the series length, is 160° of longitude (i.e., 80 points) for all latitudes. The linear trends were removed from the data as described in Section 2. This was done to decrease the possibility of leakage from wavenumbers lower than those resolvable by the basin width. The analysis was only done for the stress magnitude. This gives the distribution in wavenumber space of the kinetic energy. Initially, the log of the power spectra, $\overline{S}_m$, was plotted versus global wavenumber (GWN) and latitude for January, February, etc. (not shown). Cubic spline interpolation was used in order to obtain equidistant spacing for $\overline{S}_m$ on a logarithmic GWN scale. (The equal spacing is necessary in order to use the computer contouring subroutine.) Figs. 14 and 15 give the results for February and August, respectively, which are typical values for winter and summer. Space does not permit showing all 12 months. The GWN is also shown opposite the harmonic on all of the plots. The plots for all 12 months are presented in the appendix.

The above analysis was not performed for latitude spectra for the following reasons:

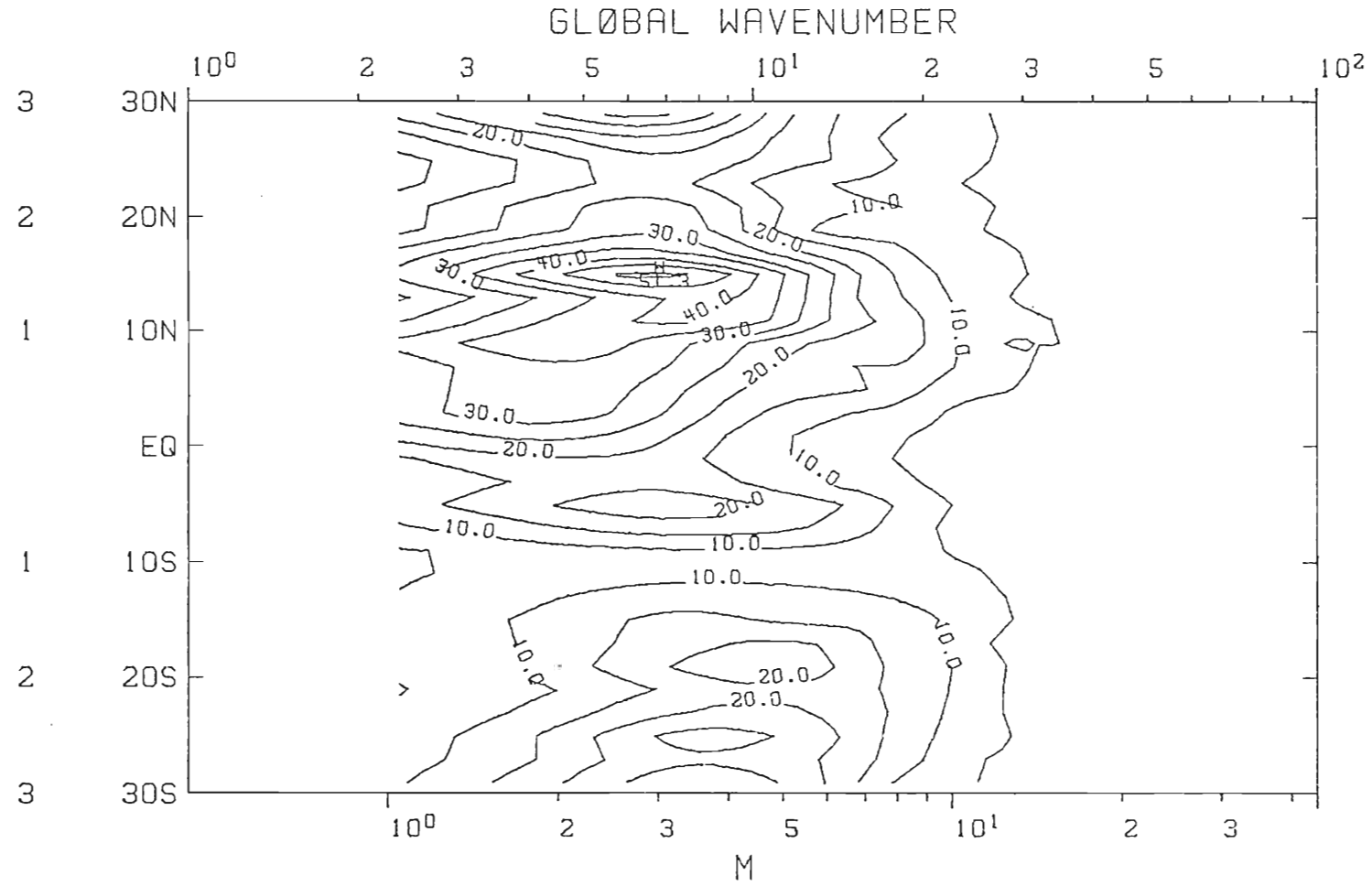

Fi Fig. 14. Wavenumber power spectra times harmonic (i.e., S_m x m) for τ, versus latitude for Febfor February. Three Hanning passes were performed on the averaged spectral estimates prior to plotto plotting. The first harmonic, and GWN = 2.25, represent a wavelength of 160° of longitude. The conThe contour interval is $5(m^4\ s^{-4})$(degrees) x 10^3.

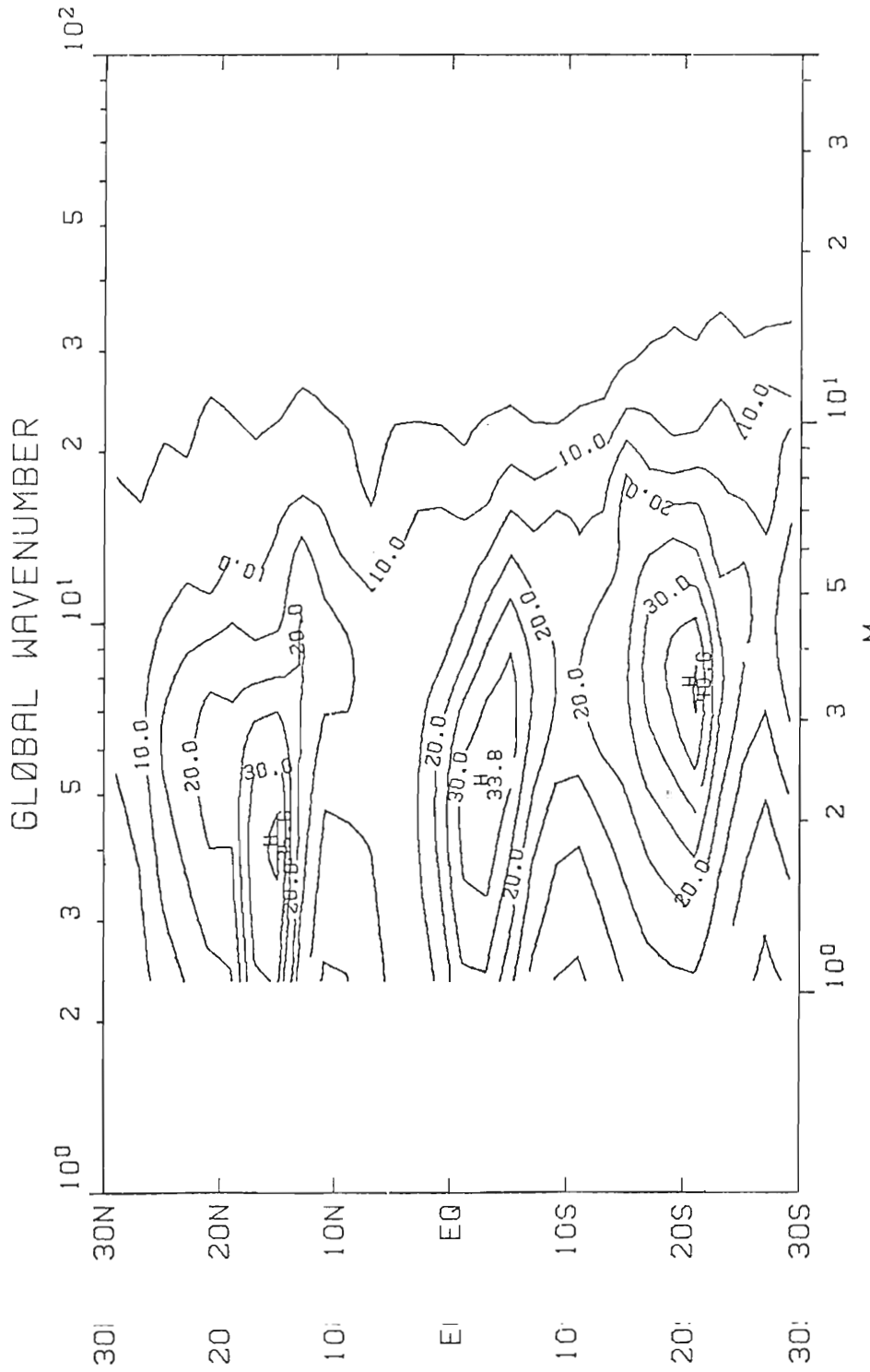

Fig. 15. Same as Fig. 14, except for August.

1) The data does not have a very broad band in the north-south direction (i.e., only 60°, or GWN of 6).

2) Trigonometric functions do not describe the field as accurately as say, spherical harmonics. However, because the data coverage was poor in the Southern Hemisphere, a spherical harmonic analysis was not attempted.

The plots of log $\overline{S}_m$ demonstrated the expected red spectra with no statistically significant peaks for all 12 months. However, the slopes vary with latitude and month. More than 95 percent of the spatial variance is associated with GWN < 18. On the average, this is the highest GWN that could be resolved by the original data (i.e., 20° of longitude).

One of the most interesting features of the plots for $\overline{S}_m m$ (i.e., Figs. 14 and 15) is that they are latitudinally coherent. This is in spite of the fact that a subjective analysis technique was used to create the data set, and that the spectral analysis was performed separately for each latitude band. Other features are the large peaks which appear at 29°N and 15°N. There are several small peaks in the Southern Hemisphere. The peaks signify that the spatial variability is concentrated in certain GWN bands. For the Northern Hemisphere peaks, the variance is concentrated between GWN 3-12. The peak at 29°N is obviously due to the variability in winter storms. The peak is present from December to March, and is the strongest in February. The maximum which is located at 15°N during February also varies throughout the year. During some months, it spreads over 5° of latitude, or splits into two maxima. The center of the peak varies from GWN 3½-7, favoring lower GWN in spring and summer. The feature is probably the result of a combination of

effects such as the southeast Asian and Central American monsoons (Wyrtki and Meyers, 1976), the core of maximum winds for the northeast trades, and the ITCZ. Tropical disturbances might also affect the results here. However, the observations of strong winds during hurricanes were eliminated when the data was originally processed (Wyrtki and Meyers, 1975a).

The hemispheric differences might be due to poor data coverage, as well as to the differences in seasons. Of course, there are major climatological asymmetries between the wind fields of the North and South Pacific; the ITCZ remains north of the equator throughout the year, the northeast trades have a larger mean and higher seasonal variability than the southeast trades (Wyrtki and Meyers, 1975a, b), and the monsoon circulation of southeast Asia covers a larger area and has higher annual variations than the Australian monsoon. These features and others, are evident in the distributions of the energy for the annual and semiannual cycles that were discussed in Section 4. The reader can draw his own conclusions about the wavenumber spectra for the Southern Hemisphere.

6. ARE THE WIND STRESS SPECTRA WHITE FOR LOW FREQUENCIES?

This section will attempt to answer the question of whether or not the wind stress frequency spectra are white for interannual periods. This is an important problem, because some ocean climate models depend on the supposition that the spectra are white for low frequencies (Frankignoul and Müller, 1979). The frequency spectra for the spatially averaged zonal wind stress of the northeast and southeast trades for 1948-1972, were calculated by Wyrtki and Meyers (1976). Their results show no significant peak for interannual periods. However, the coherency between the trades increases above the 95 percent confidence limit for the lowest frequencies. It is obvious that the significance of the results of the test used in this study will be inhibited by the even shorter record length of 10 years. However, as with the discussion in Section 4 of the total low frequency energy, the results reveal interesting distributions, even though their statistical reliability is small.

The Kolmogorov-Smirnov goodness-of-fit test (K-S test) is used at each point to evaluate the null hypothesis that the spectrum for low frequencies is white (Jenkins and Watts, 1969). The test uses the integrated spectrum as a cumulative distribution function. The maximum absolute deviation from the theoretical distribution is called D_{max}. This is compared to a critical value, D_{crit}, for a particular level of

This is compared to a critical value, D_{crit}, for a particular level of

significance. The significance level for this study was chosen to be 20 percent. Spectral estimates for periods greater than or equal to 120/7 months, i.e., the first seven harmonics, were used to construct the integrated spectrum. In this type of test, the last estimate, i.e., the highest frequency used, does not affect the results. Therefore, just as for the discussion of the total low frequency energy in Section 4, only the spectral estimates for periods $\geq$ 20 months are actually being tested for whiteness. For the purpose of this test, the linear trend was removed from the time series at each point before the spectral estimates were computed.

The test was performed on the unsmoothed, low frequency spectra for τ, τ_x and τ_y. The value used for D_{crit} was .410 (Ostle, 1963). However, the resultant number of points which failed the test for the hypothesis appeared to be too small. Less than 12 percent of the points tested for τ, τ_x and τ_y failed the test. Even if the spectral estimates were from a white noise process, approximately 20 percent of the points should have failed the test because of the 20 percent significance level. In order to verify this, random χ^2 variables with two degrees of freedom were generated. If $0 < x < 1$ is a random number with a uniform distribution function, then $\chi^2 = -2\log x$ is a chi-square variable with 2 degrees of freedom. The random variables were used to simulate the raw spectral estimates of a white noise process. When the same K-S test was performed on the random data, only about 13 percent of the points failed the null hypothesis. Thus, either the values from the table are incorrect for this application, or the sample size of seven estimates at each
the null hypothesis. Thus, either the values from the table are incorrect for this application, or the sample size of seven estimates at each
point is too small for the type of test being used.

A new critical value was calculated by first creating a probability density distribution from the values of D_{max} calculated above when the randomly generated χ^2 variables were used. The K-S test was run for 2155 points. This was a sufficient number for a good probability density distribution. The 20 percent level was found to be associated with $D_{crit} = .373$. The K-S test was then repeated on the low frequency spectra for τ, τ_x and τ_y, with the new empirical value for D_{crit}. Of the 2155 points, 19 percent failed the null hypothesis for τ, and 18 percent of the points failed for both τ_x and τ_y. These values are approximately what would be expected if the process was indeed white noise. However, the spatial distributions of the points which failed the K-S test are of interest and deserve further discussion.

Fig. 16 shows the results for τ and for the randomly generated χ^2 variables. As would be expected, the points at which the χ^2 variables are significant appear to be random. There are some areas for the τ distribution that are more densely covered than others. These include:

1) The region in the eastern half of the South Pacific from about 11-23°S. This is part of the region occupied by the Walker Circulation (Walker, 1923; Bjerknes, 1969; Julian and Chervin, 1978).

2) The region in the North Pacific from about 140-178°E. This area is associated with the southeast Asian monsoon circulation.

3) The area surrounding the average position of the ITCZ (~ 10°N) in the central North Pacific.

In addition, the distribution for τ_x (not shown) includes a region of

in the central North Pacific.

In addition, the distribution for τ_x (not shown) includes a region of dense coverage north of 23°N from about 155°E-170°W. This would be

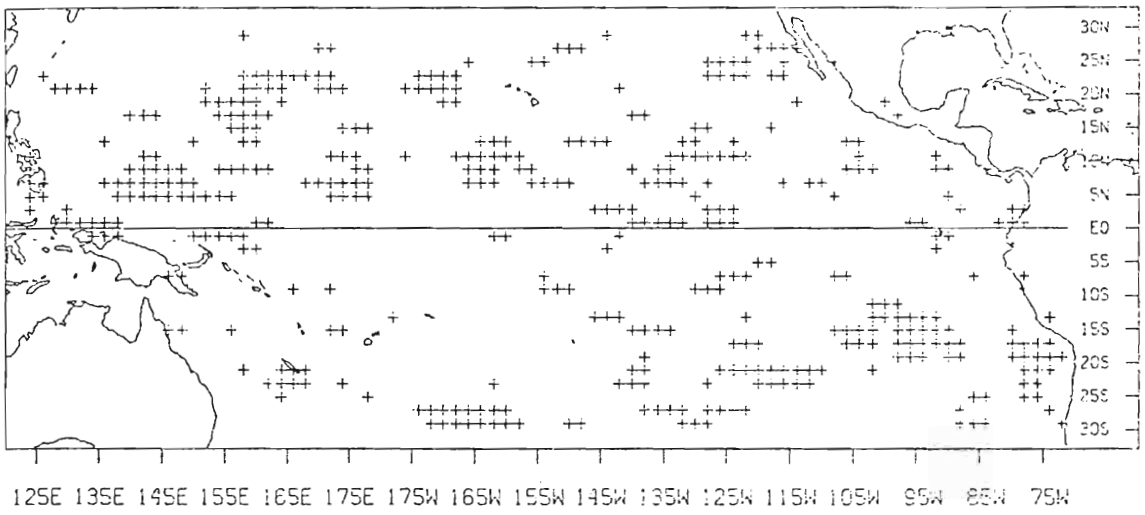

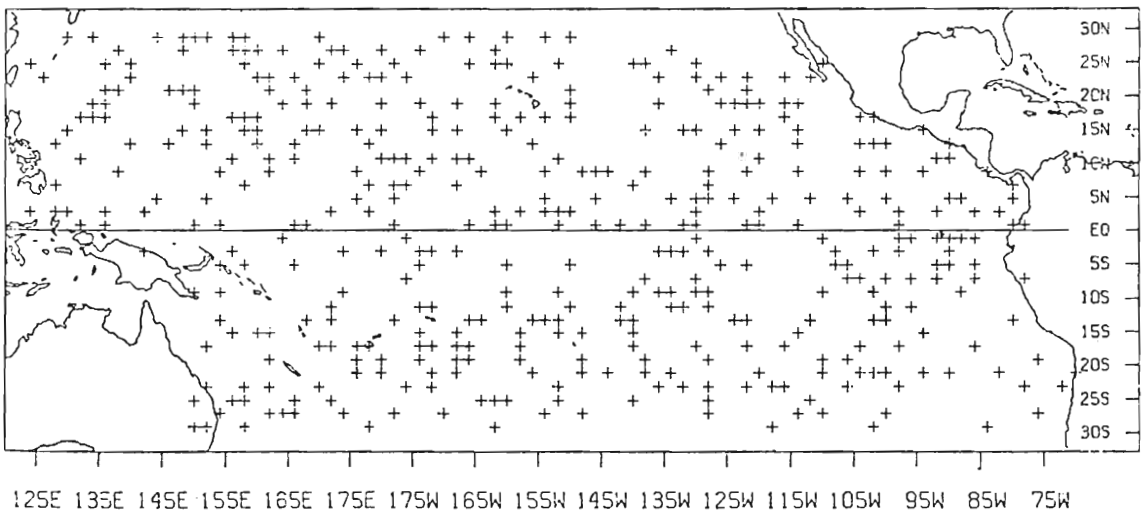

Fig. 16. Results of the K-S test for white noise for (a) τ and (b)χ^2 r.v. with two degrees of freedom. Points which failed the null hypothesis at the 20 percent significance level are indicated by +.

(b)χ^2 r.v. with two degrees of freedom. Points which failed the null hypothesis at the 20 percent significance level are indicated by +.

associated with the interannual variation of winter storm tracks discussed in Section 4. The distribution for τ_y (not shown) contains one additional area, just off the east coast of Australia. The density of the patterns can be deceiving however. This is because, as discussed previously in Sections 3 and 4, the neighboring points are not truly independent. Five longitudinal points were created for every point of the original data. Thus, east-west bands of up to five points should not be considered significant. The above discussion does not apply to adjacent points in the north-south direction.

The tentative conclusion for the results of this section is that the wind stress spectra are white for low frequencies. However, the patterns of the points which fail the test are intriguing and should be rechecked with longer data sets.

7. SUMMARY AND CONCLUSIONS

Ship wind observations, averaged month by month for 2° x 10° latitude-longitude boxes by Wyrtki and Meyers (1975a, b, 1976), are subjectively analyzed to provide monthly maps of wind stress for the decade 1961-1970 on a 2° x 2° grid over the tropical Pacific. Frequency and seasonal zonal wavenumber spectra are calculated. The results reveal that the frequency spectra vary greatly from region to region. Only the annual and semiannual peaks are statistically significant using 80 percent confidence limits.

The subjective analysis techniques used for this study are briefly compared with two objective analysis techniques: the method of empirical orthogonal functions (EOF) (Barnett, 1977a) and the method of successive corrections (Goldenberg, 1979, unpublished manuscript). The spatial smoothing is greater in both of the objective methods than for the subjective analysis. The latitudinal smoothing used in the EOF approach could have the effect of decreasing the accuracy of north-south derivatives. The other differences are in the techniques used to fill in the data void regions. It is doubtful that any of these variations would contribute to significant differences in the spectral analysis of the present study.

Frequency spectra of the wind stress allow an examination of the time scales 2 months to 10 years. The spectra vary greatly between

Frequency spectra of the wind stress allow an examination of the time scales 2 months to 10 years. The spectra vary greatly between

the wind stress magnitude, τ, and the wind stress components, τ_x and τ_y. The spectra for a large portion of the tropical Pacific display a pronounced annual signal, which is typically strongest for the zonal component, τ_x. It is demonstrated how the annual variability for τ_x and τ_y can be "folded" into the semiannual time scale in τ. These differences between the wind stress magnitude and the components can be important when looking at the oceanic response to the winds for different types of ocean models.

Distributions for annual and semiannual variability clearly show the well-known climatological features: the monsoon circulations of southeast Asia and North Australia, wintertime intrusion of mid-latitude storms into the subtropical Pacific, seasonal variations in the position of the ITCZ and the oscillation in the strength of the northeast trades.

The 10 year record length of the present study is too short to accurately resolve interannual variability. As an alternative, the distribution of the total energy for all periods 20 months and longer is plotted. There are three areas of high interannual variability: a band stretching from Chile to Australia, a region over the central equatorial Pacific and a region poleward of 21°N in the central Pacific. The first area is located in the region where the Southern Oscillation (SO) index is measured. The SO index has been used to predict El Niño occurrences (Quinn, 1974; Wyrtki, et al., 1976). The second area is believed to be the key area in the Kelvin wave mechanism which causes El Niño. A 12-month running mean for this last area clearly shows a relaxation in the southeast trades, occurring several months prior to each of the three El Niño events of the Sixties. These results are fur-

ther confirmations of the theory of El Niño, originally developed by Wyrtki (1975). The third area is associated with interannual variability in the intensity of the mid-latitude winter storms which influence the subtropics. Of particular interest, is the apparent positive correlation between the strength of those storms and the strength of the southeast trades of the Southern Hemisphere. Future research could examine this association further.

The monthly zonal wavenumber spectra are red, as expected. The spatial variability is concentrated in global wavenumber 3-12, particularly in the latitudes influenced by winter storms, containing the ITCZ or the cores of the maximum trade winds. More than 95 percent of the variance is contained in the spatial scales resolvable by the original data (i.e., 20° of longitude). Additional research could study the frequency-wavenumber spectra to investigate the distribution of spatial atmospheric variability as a function of frequency.

The last part of the present study employs the Kolmogorov-Smirnov goodness-of-fit test to examine the low frequency spectra for whiteness. A new empirical critical value is used for the test at the 20 percent significance level. The results confirm earlier studies that the wind spectra are white for interannual periods. However, the regions where points failed the test for white noise are of special interest, such as the area associated with the Walker circulation (Walker, 1923). It would be desirable to further investigate the low frequency spectra when longer data sets are made available.

The purpose of this study is to provide a better insight into the frequency spectra when longer data sets are made available.

The purpose of this study is to provide a better insight into the distribution of time and space variability of the wind stress. It is

hoped that the results can be used to further investigate the oceanic response to the seasonal and interannual atmospheric forcing. With a data set as this, there are considerable more analyses that could be performed. The data are available for other investigators.

APPENDIX

Monthly Zonal

Wavenumber Spectra

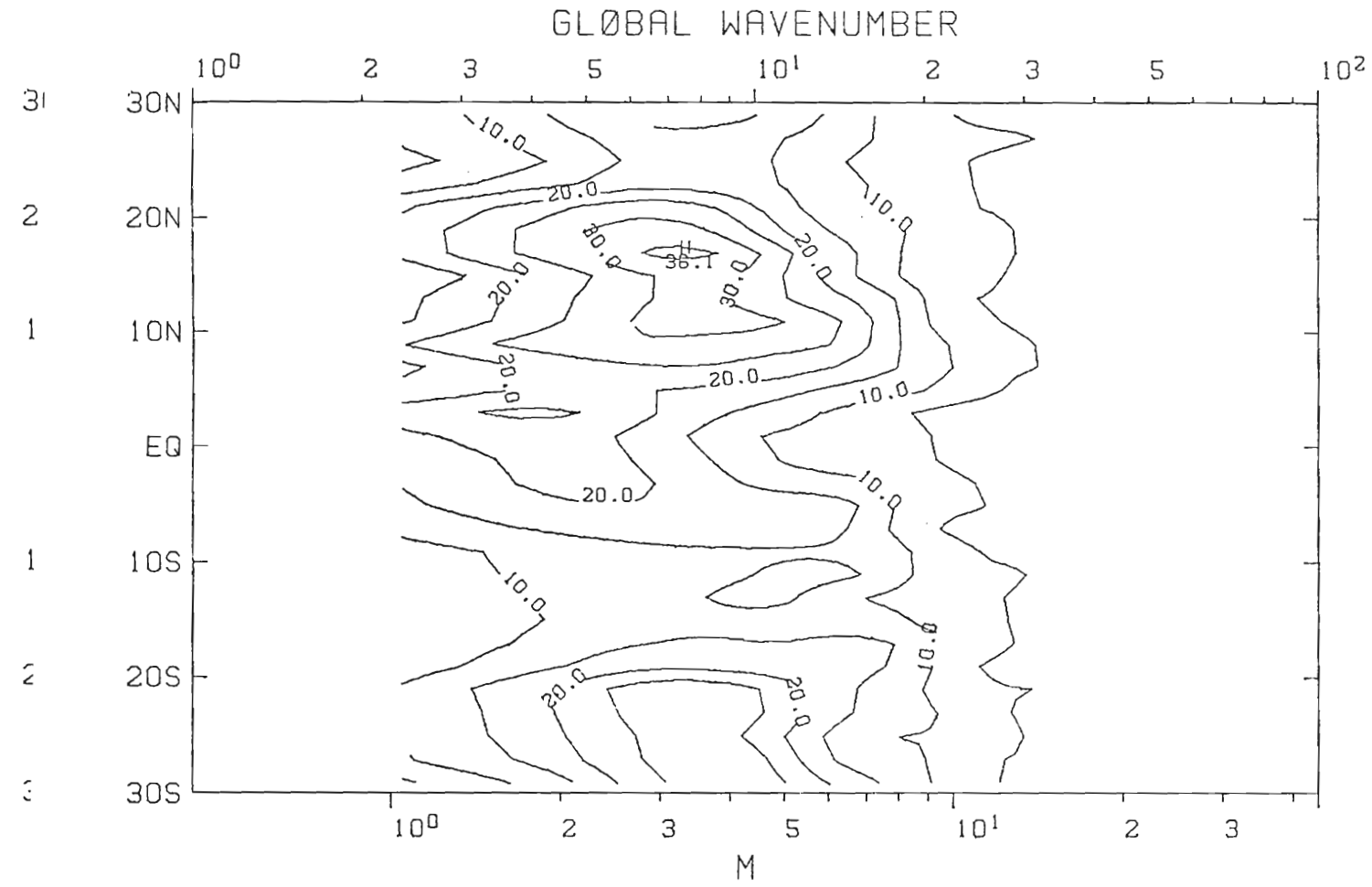

Al Al. Same as Fig. 14, except for January.

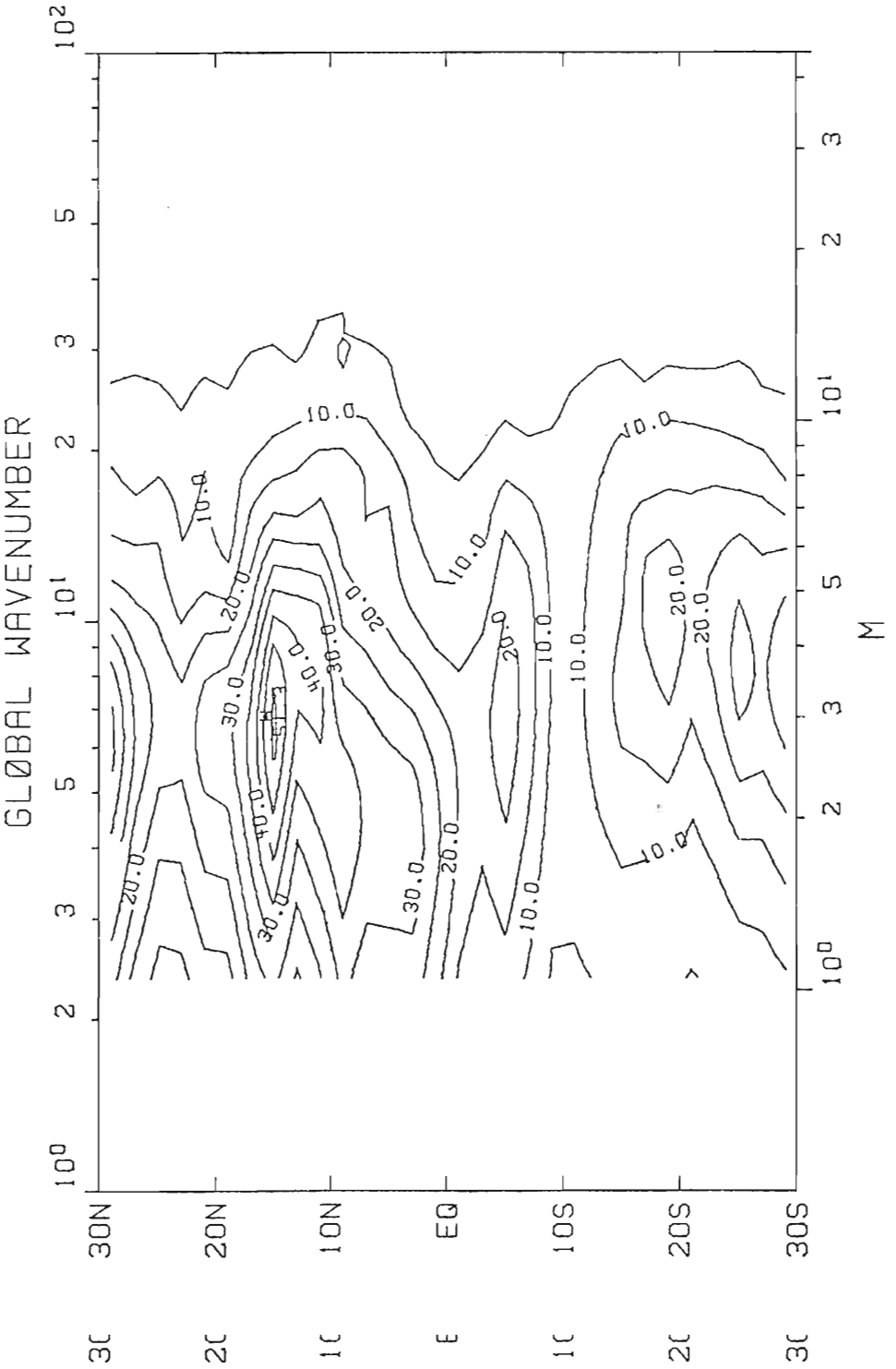

A2. Same as Fig. 14.

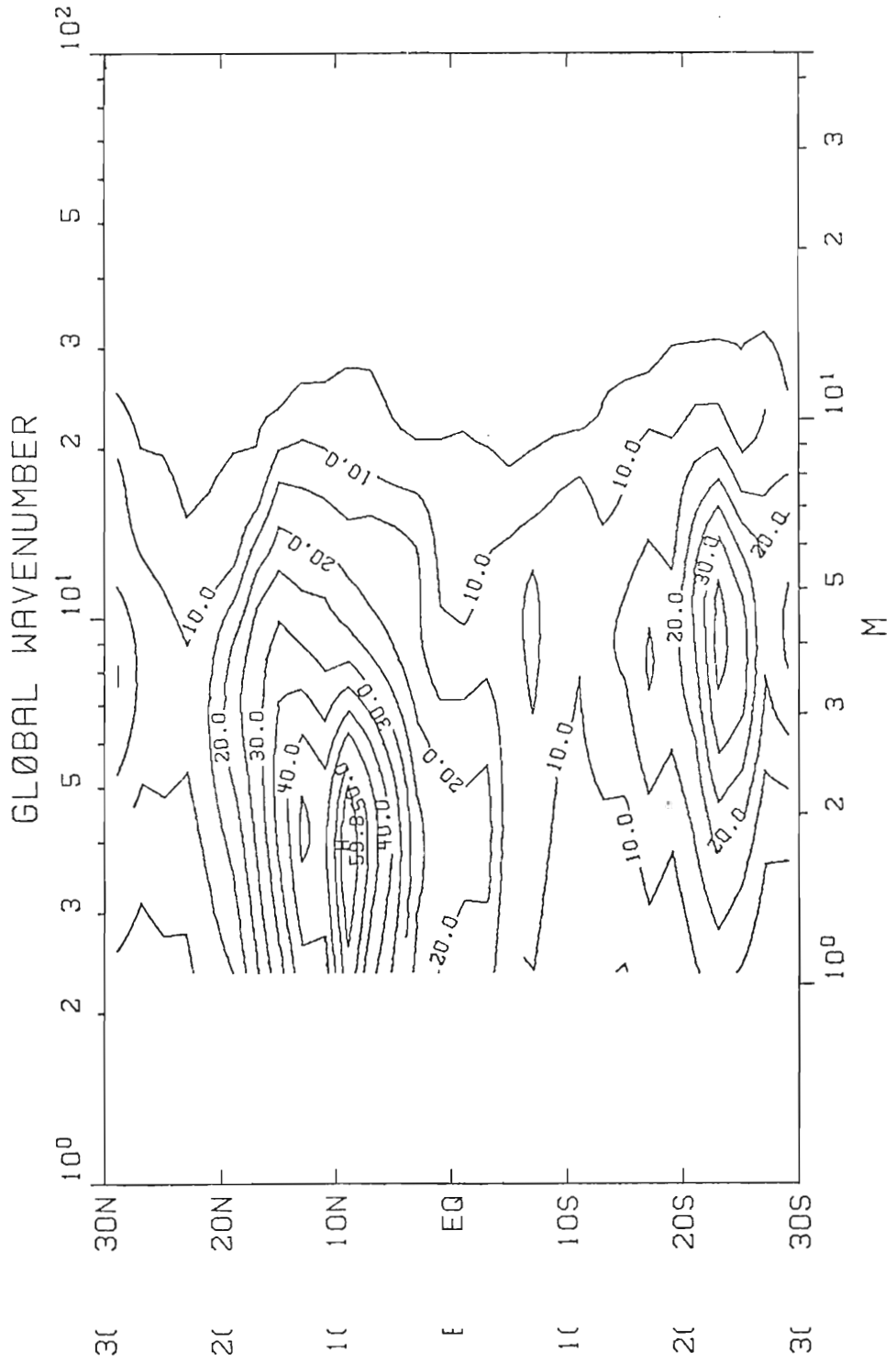

A3. Same as Fig. 14, except for March.

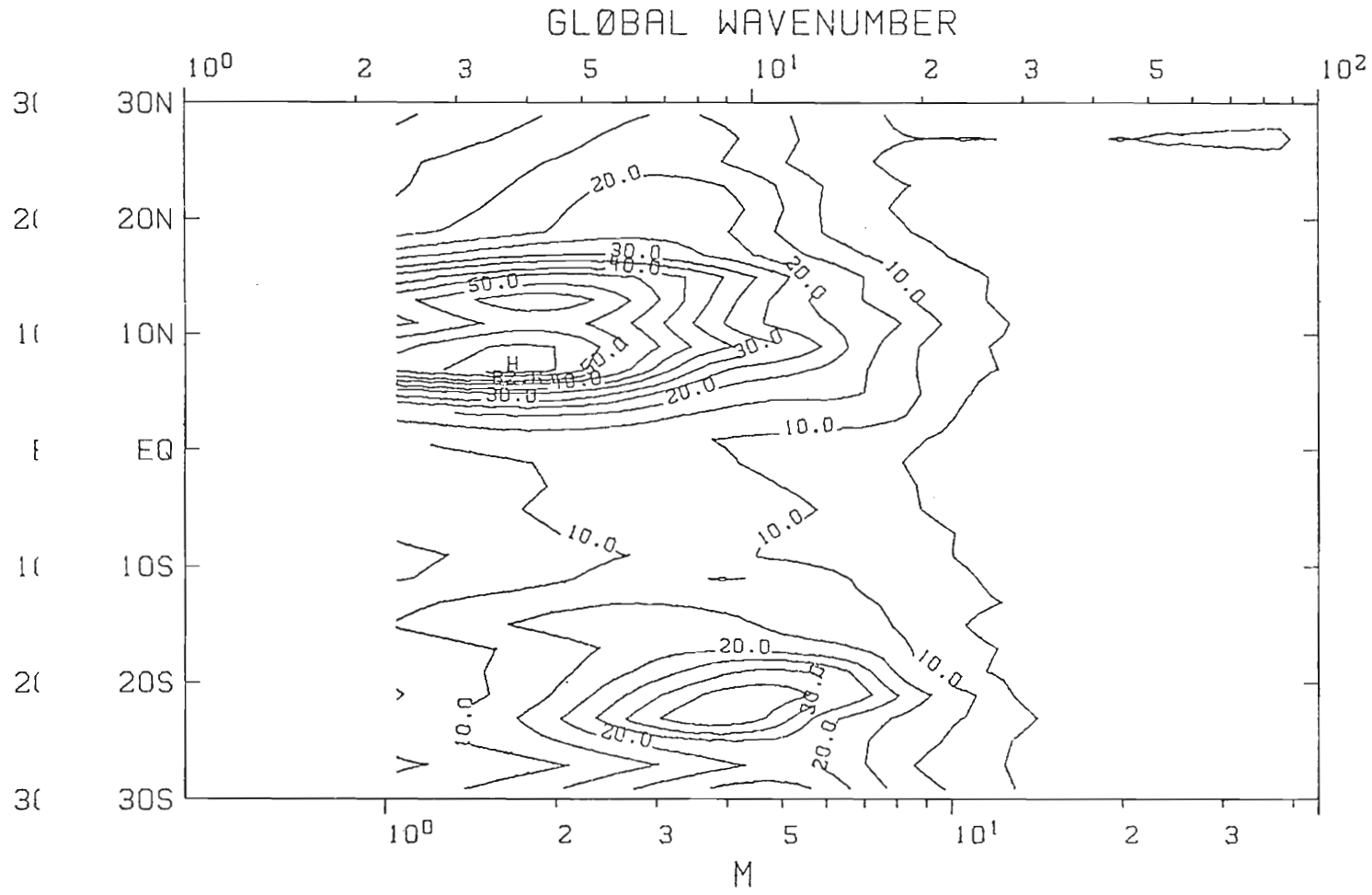

A4. A4. Same as Fig. 14, except for April.

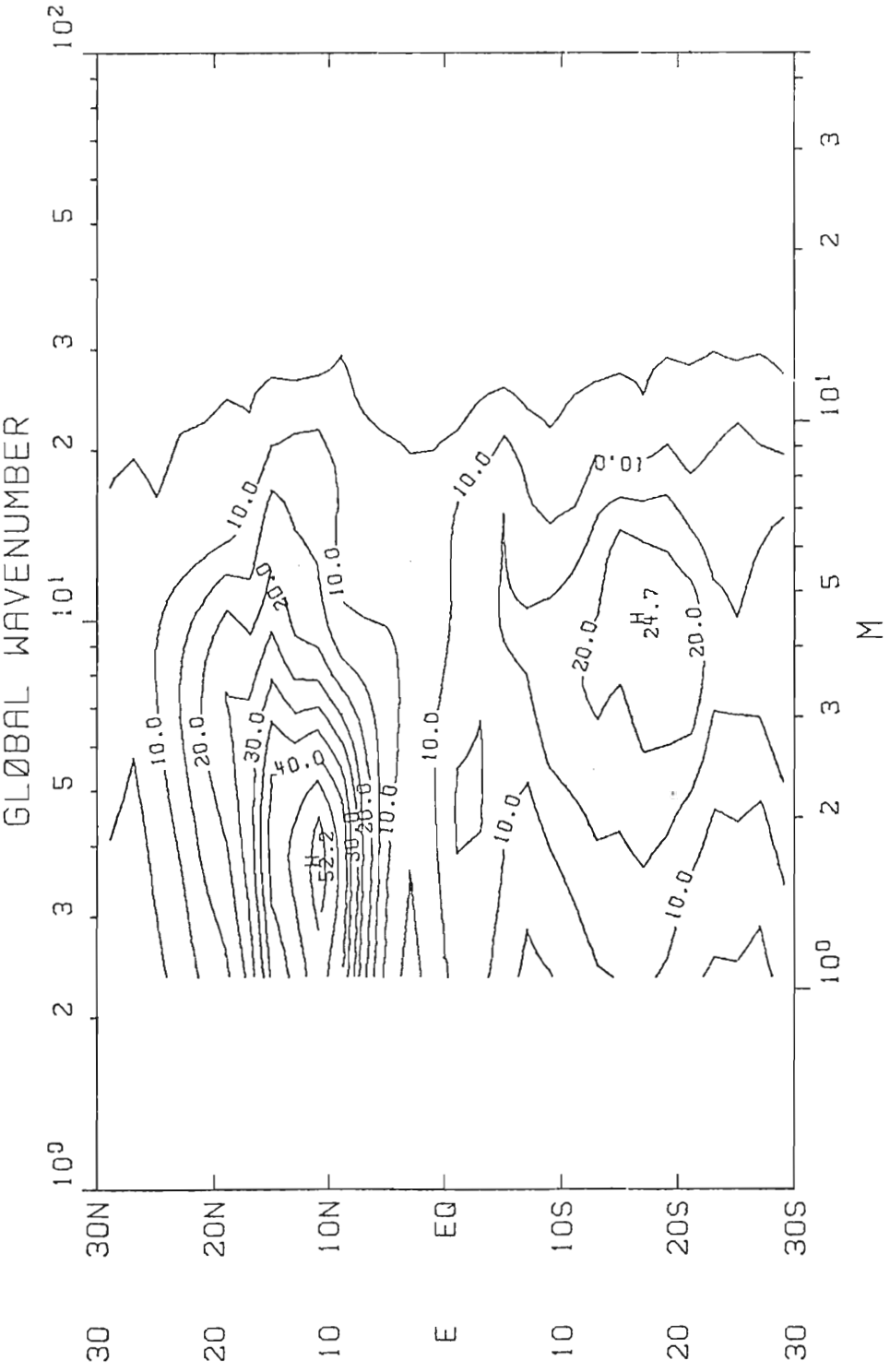

A5. Same as Fig. 14, except for May.

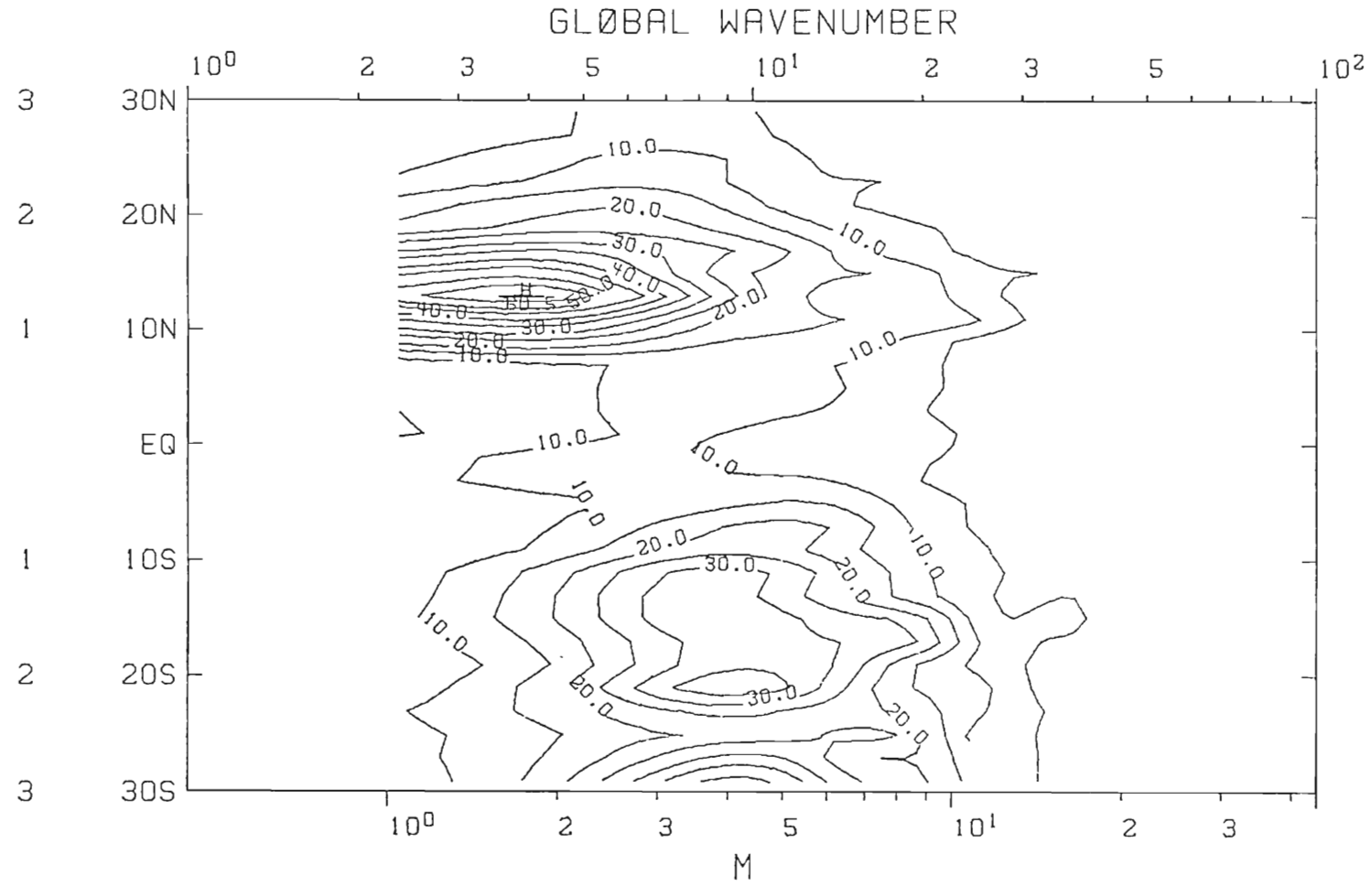

A6. A6. Same as Fig. 14, except for June.

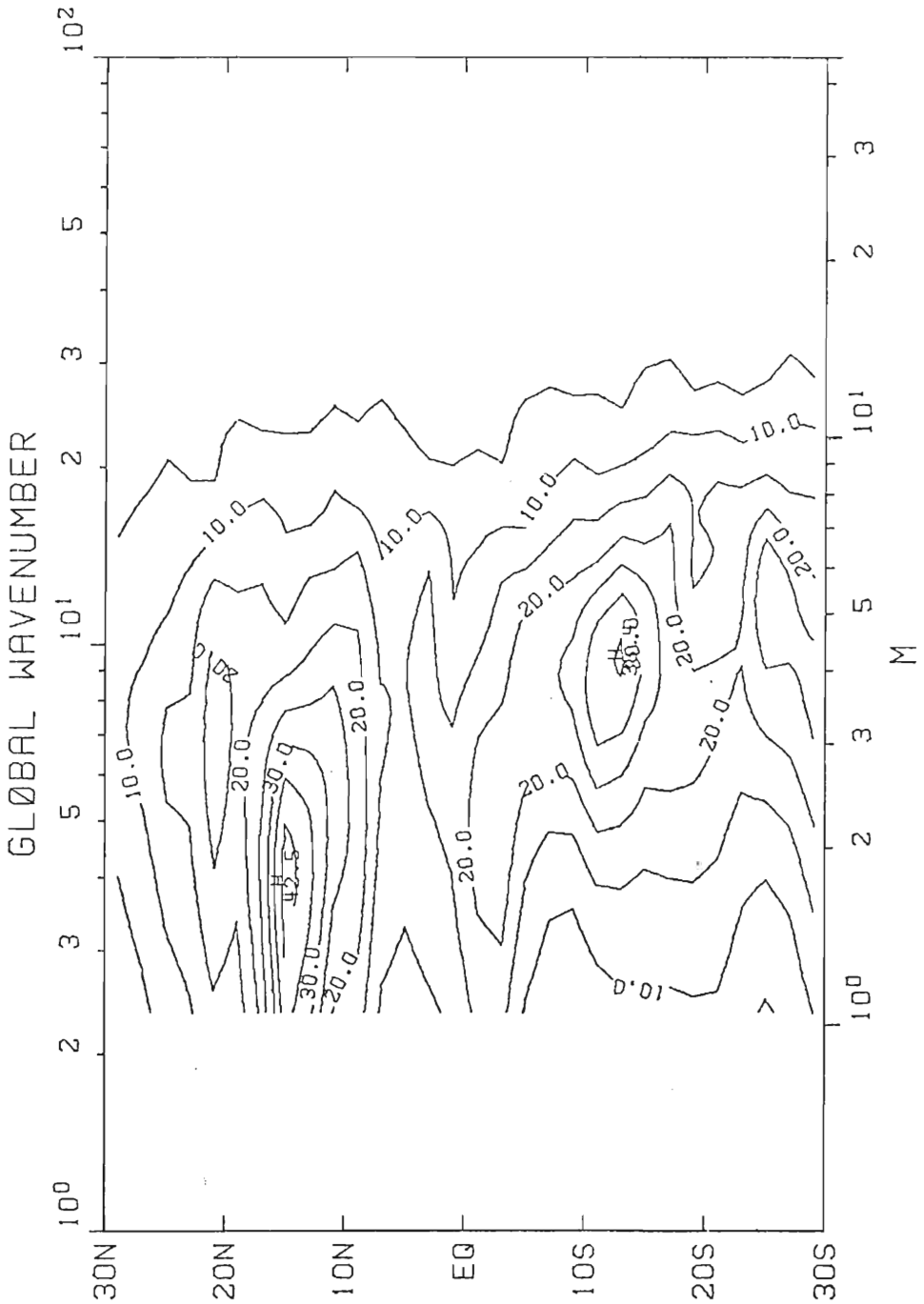

A7. Same as Fig. 14, except for July.

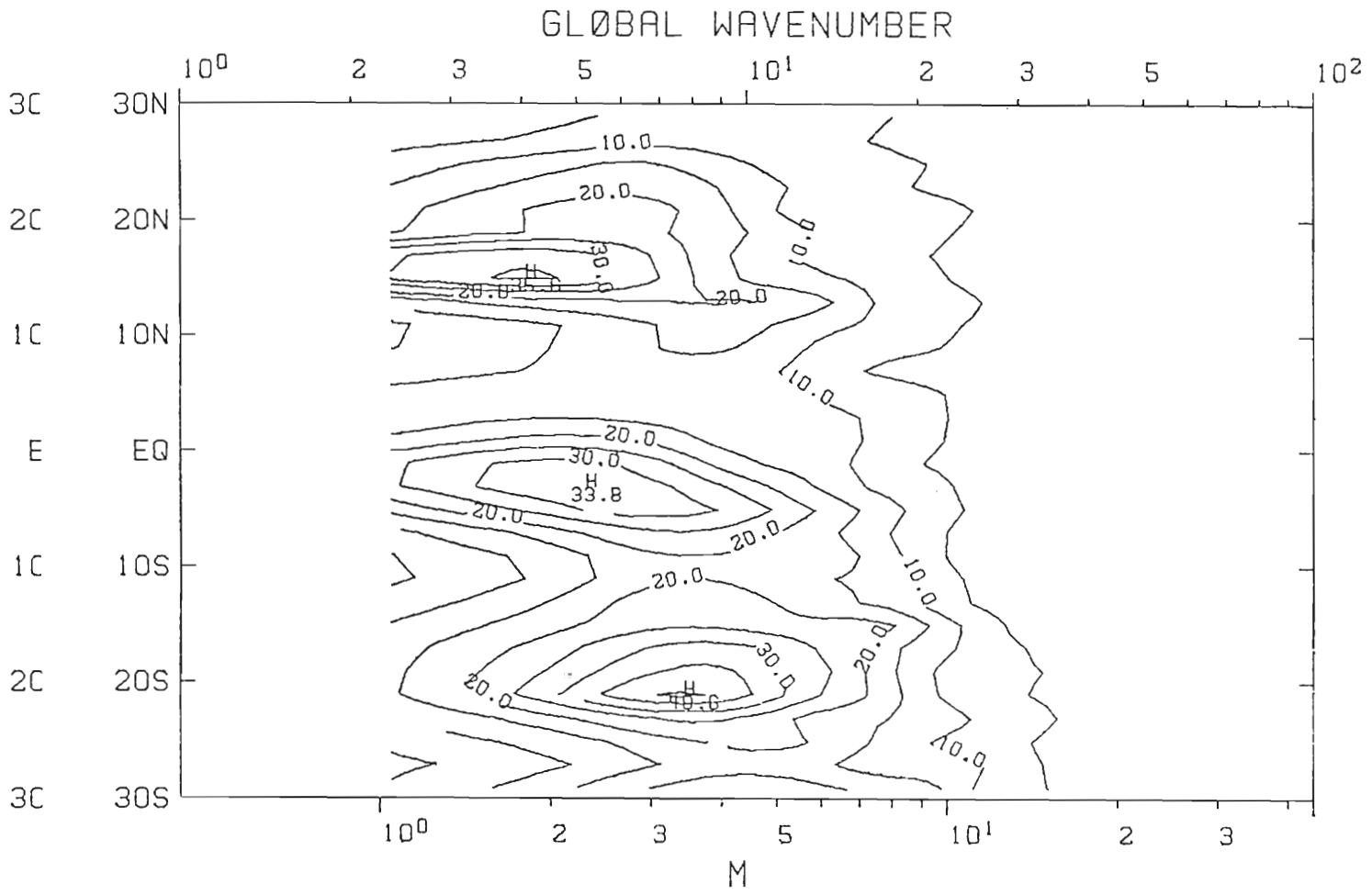

A8. A8. Same as Fig. 14, except for August.

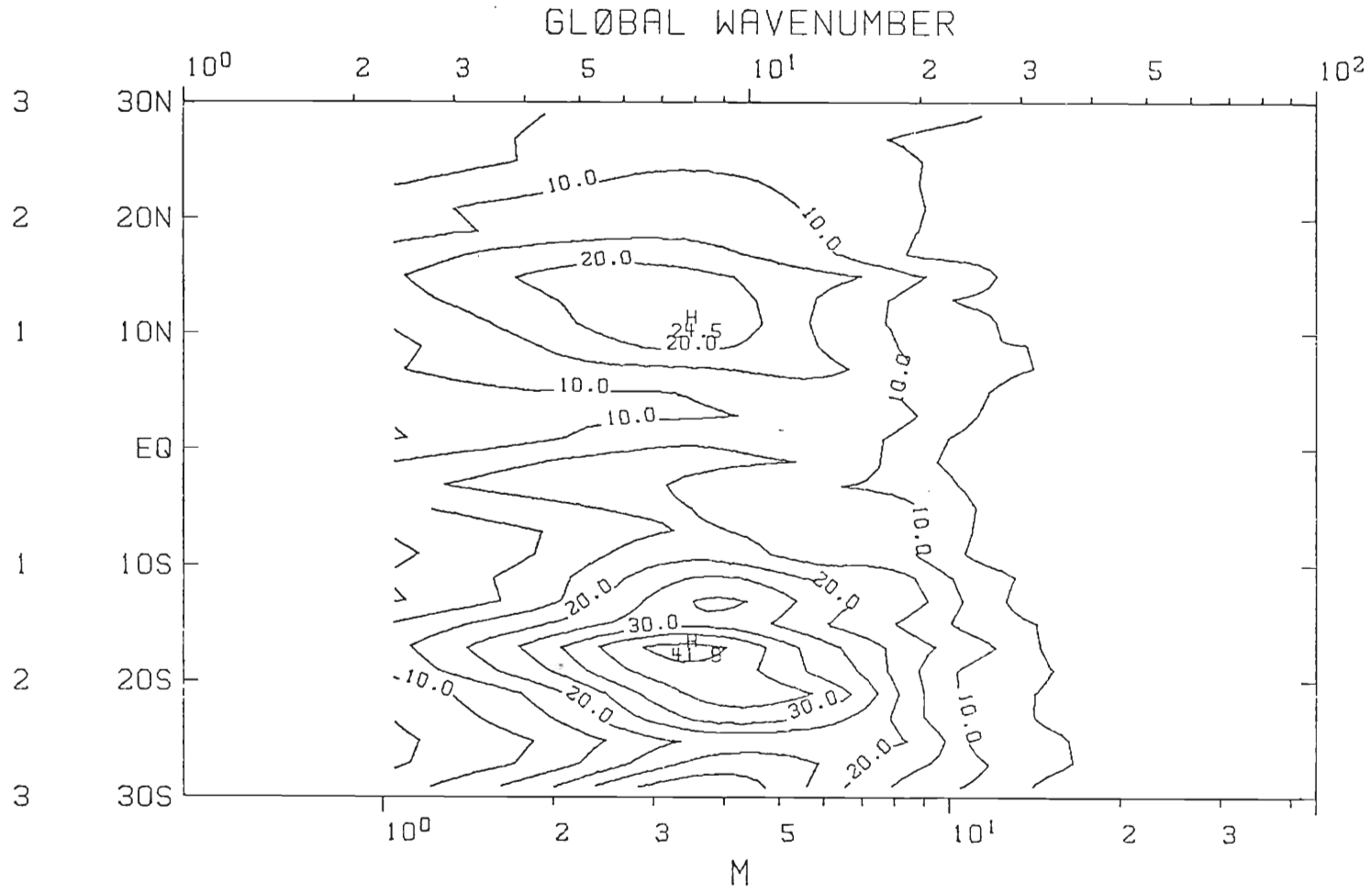

A9 A9. Same as Fig. 14, except for September.

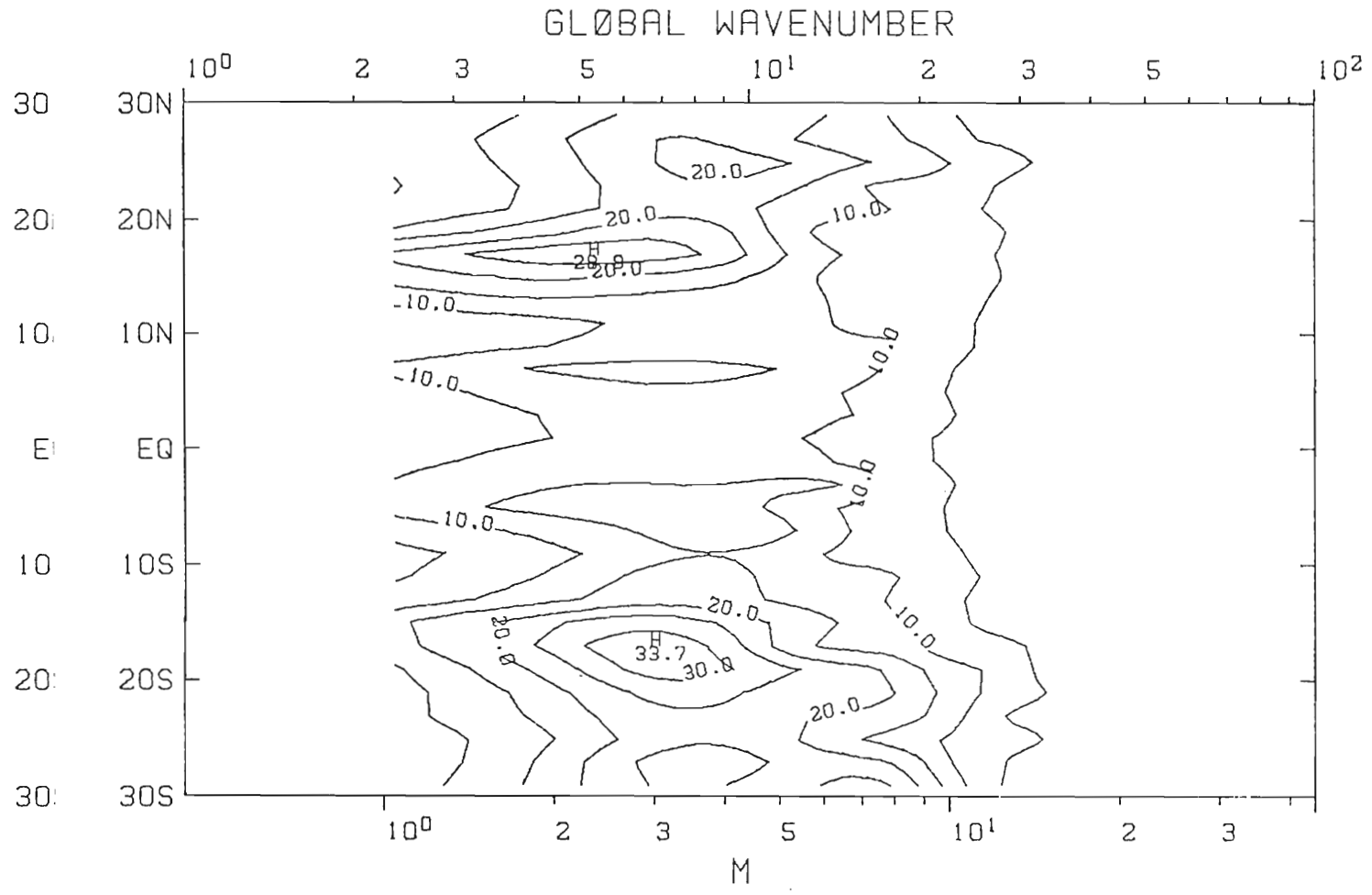

A10. Same as Fig. 14, except for October.

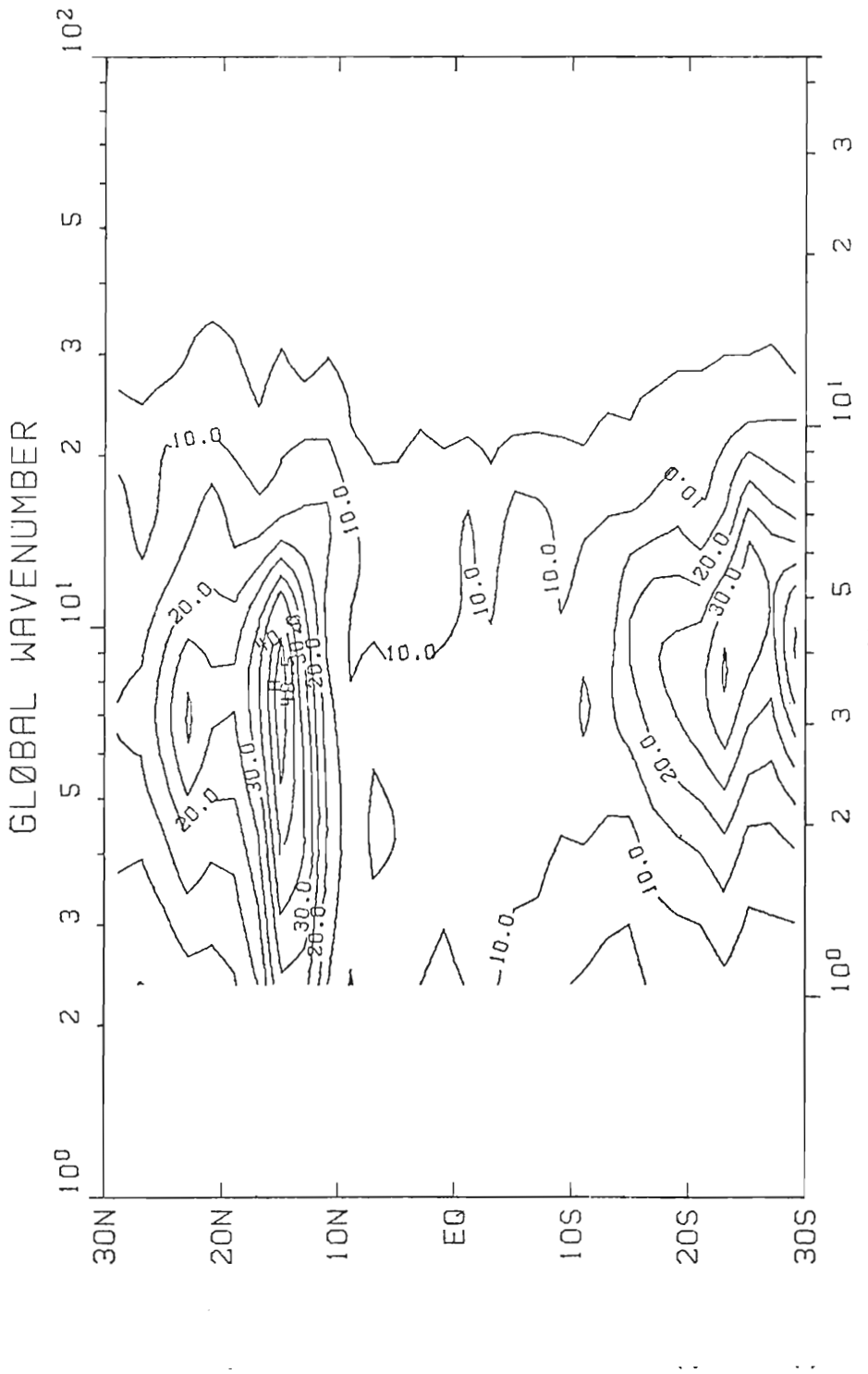

All. Same as Fig. 14, except for November.

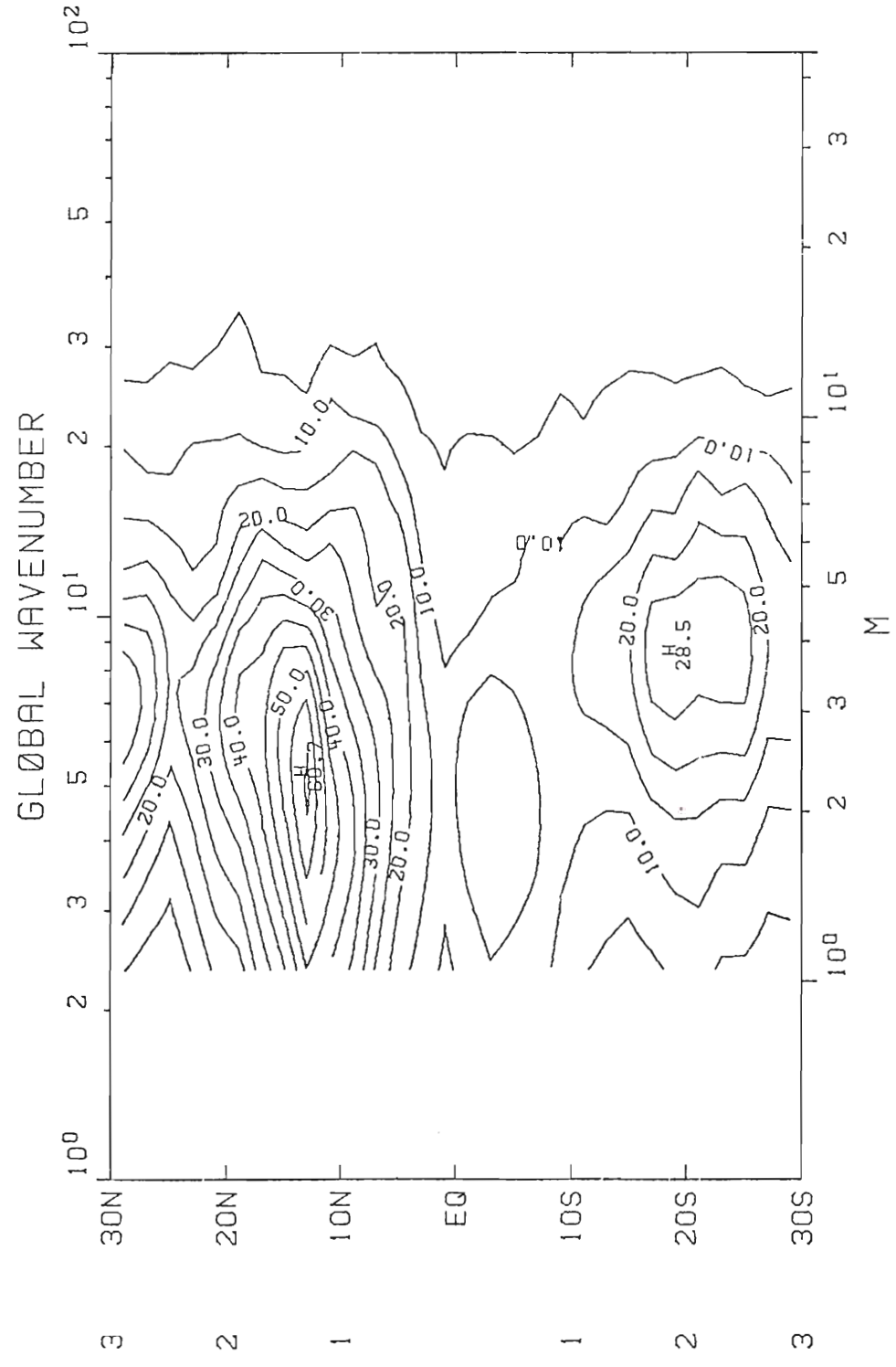

A1 A12. Same as Fig. 14, except for December.

REFERENCES

Atkinson, G.D., 1971: Forecaster's Guide to Tropical Meteorology, Air Weather Service, USAF.

Barnett, T.P., 1977a: The principal time and space scales of the Pacific trade wind fields. J. Atmos. Sci., 34, 221-236.

_____, 1977b: An attempt to verify some theories of El Niño, J. Phys. Oceanogr., 7, 633-647.

Bergthorsson, P., and Döös, B., 1955: Numerical weather-map analysis. Tellus, 7, 329-340.

Bjerknes, J., 1966: Survey of El Niño 1957-58 in its relation to tropical Pacific meteorology. Inter-Amer. Trop. Tuna Comm. Bull., 12, 62 pp.

_____, 1969: Atmospheric teleconnections from the equatorial Pacific. Mon. Wea. Rev., 97, 163-172.

Cressman, G.P., 1959: An operational objective analysis system. Mon. Wea. Rev., 87, 367-374.

Frankignoul, C., and P. Müller, 1979: Quasi-geostrophic response of an infinite β-plane ocean to stochastic forcing by the atmosphere. J. Phys. Oceanogr., 9, 104-127.

Hastenrath, S., and P. Lamb, 1977: Climatic atlas of the tropical Atlantic and eastern Pacific oceans. The University of Wisconsin Press, 15 pp.

Hellerman, S., 1967: An updated estimate of the wind stress on the world ocean. Mon. Wea. Rev., 95, 607-626.

Hsu, C.-P.F., and J.M. Wallace, 1976: The global distribution of the annual and semiannual cycles in sea level pressure. Mon. Wea. Rev., 104, 1597-1601.

Hurlburt, H.E., J.C. Kindle and J.J. O'Brien, 1976: A numerical simulation of the onset of El Niño. J. Phys. Oceanogr., 6, 621-631.

Hurlburt, H.E., J.C. Kindle and J.J. O'Brien, 1976: A numerical simulation of the onset of El Niño. J. Phys. Oceanogr., 6, 621-631.

Jenkins, G.M., and D.G. Watts, 1969: Spectral analysis and its applications. Holder Day, San Francisco.

Julian, P.R. and R.M. Chervin, 1978: A study of the Southern Oscillation and Walker Circulation phenomenon. Mon. Wea. Rev., 106, 1433-1451.

Kindle, J.C., 1979: Equatorial Pacific Ocean variability--seasonal and El Niño time scales. Ph.D. thesis, Florida State University.

McCreary, J., 1976: Eastern tropical ocean response to changing wind systems with application to El Niño. J. Phys. Oceanogr., 6, 632-645.

McDonald, W., 1938: Atlas of Climate Maps of the Ocean. Weather Bureau No. 1247, Govt. Printing Office, Washington, DC, 130 pp.

O'Brien, J.J., 1979: Equatorial oceanography. Rev. Geophys. Space Phys., 17, 1569-1575.

_____, A. Busalacchi and J. Kindle, 1980: Ocean models of El Niño. El Niño and the Peruvian Fishery: science, politics and economics, M. Glantz and J.D. Thompson, Eds., Wiley-Interscience (to appear).

Ostle, B., 1963: Statistics in research. The Iowa State University Press, Ames.

Quinn, W.H., 1974: Monitoring and predicting El Niño invasions. J. Appl. Meteor., 13, 825-830.

_____, and W.V. Burt, 1970: Prediction of abnormally heavy precipitation over the equatorial Pacific dry zone. J. Appl. Meteor., 9, 20-28.

_____, and W.V. Burt, 1972: Use of the Southern Oscillation in weather prediction. J. Appl. Meteor., 11, 616-628.

Reiter, E.R., 1978a: The interannual variability of the ocean-atmosphere system. J. Atmos. Sci., 35, 347-370.

_____, 1978b: Long-term wind variability in the tropical Pacific, its possible causes and effects. Mon. Wea. Rev., 106, 324-330.

Stephens, J.J., and A.L. Polan, 1970: Spectral modification by objective analysis. Mon. Wea. Rev., 99, 374-378.

Walker, G.T., 1923: Correlation in seasonal variations of weather VIII. Mem. Indian Meteor. Dept., 24, 75-131.

Walker, G.T., 1923: Correlation in seasonal variations of weather VIII. Mem. Indian Meteor. Dept., 24, 75-131.

Willebrand, J., 1978: Temporal and spatial scales of the wind field over the North Pacific and North Atlantic. J. Phys. Oceanogr., 8, 1080-1094.

Wyrtki, K., 1975: El Niño--The dynamic response of the equatorial Pacific Ocean to atmospheric forcing. J. Phys. Oceanogr., 5, 572-584.

_____, and G. Meyers, 1975a: The trade wind field over the Pacific Ocean. Part I. The mean field and the mean annual variation. Rep. HIG-75-1. Hawaii Inst. Geophys., University of Hawaii, 26 pp.

_____, and _____, 1975b: The trade wind field over the Pacific Ocean. Part II. Bimonthly fields of wind stress: 1950 to 1972. Rep. HIG-75-2, Hawaii Inst. Geophys., University of Hawaii, 16 pp.

_____, and _____, 1976: The trade wind field over the Pacific Ocean. J. Appl. Meteor., 15, 698-704.

_____, E. Stroup, W. Patzert, R. Williams and W. Quinn, 1976: Predicting and observing El Niño. Science, 191, 343-346.